J. Fluid Mech. (1989), *vol.* 205, *pp.* 99–133
Printed in Great Britain

Scalar transport and alpha-effect for a family of cat's-eye flows

By S. CHILDRESS[1] AND A. M. SOWARD[2]

[1] Courant Institute of Mathematical Sciences, 251 Mercer Street, New York, NY 10012, USA
[2] School of Mathematics, The University, Newcastle upon Tyne, NE1 7RU, UK

(Received 7 March 1988 and in revised form 3 February 1989)

In this paper we study advection–diffusion of scalar and vector fields for the steady velocity field

$$(u, v, w) = \left(\frac{\partial \psi}{\partial y}, -\frac{\partial \psi}{\partial x}, K\psi\right), \quad \psi = \sin x \sin y + \delta \cos x \cos y.$$

If $\delta > 0$ the streamlines $\psi =$ constant form a periodic array of oblique cat's-eyes separated by continuous channels carrying finite fluid flux. In the problems treated, advection dominates diffusion, and fields are transported both in thin boundary layers and within the channels. Effective transport of a passive scalar and the alpha-effect generated by interaction of the flow with a uniform magnetic field are examined. For the latter problem, we determine the alpha-matrix as a function of δ. Our results consist of (i) numerical solution of steady problems in the limit of large Reynolds number R with $\beta = \delta R^{\frac{1}{2}}$ held fixed and $O(1)$, and (ii) analytic asymptotic solutions for large R, obtained using the Wiener–Hopf technique, which are valid for large β. The asymptotic method gives reliable values of the effective diffusion and of alpha-matrices down to $\beta \approx 1.5$.

When $\beta > 0$ the transport and alpha-effect are greatly enhanced by flux down the channels. Consequently, the alpha-effect found here may have application to the construction of efficient fast dynamos, but this requires spatial dependence of the mean field and the inclusion of three-dimensional effects, as in the established fast-dynamo analysis with $\delta = 0$.

1. Introduction

1.1. *The scope of the paper*

A central problem of fluid kinematics concerns the advection and diffusion of passive scalar and vector fields in a given flow $\boldsymbol{u}(\boldsymbol{x}, t)$. Problems of this kind arise in the calculation of average transport of a scalar field as a result of a fixed mean gradient and, for the case of an electrically conducting fluid, in the construction of kinematic dynamos utilizing an alpha-effect (as reviewed in e.g. Moffatt 1978). In many problems of interest, moreover, advection is much stronger than diffusion, and the bulk properties of interest may arise in part from many small regions where diffusion is non-negligible. The calculation of the bulk properties from their 'microscopic' origins is a notoriously difficult problem, turbulent diffusion at high Reynolds number being the extreme case.

The simplest class of such problems is obtained when $\boldsymbol{u}$ is independent of time. Even for steady flows, the limit of large Reynolds number is not a simple one, because of the existence of diffusive boundary layers in the neighbourhood of certain

lines and surfaces. We shall, in the present paper, consider only the steady case. We shall study advection–diffusion for a steady flow which is independent of one coordinate (z), but which (if the parameter K below is non-zero) has a non-trivial three-dimensional streamline pattern. In particular, when advection is dominant, there will exist a complicated set of boundary layers, localized near surfaces in three-dimensional space.

The flow field is a one-parameter extension of a symmetric square-cell geometry, considered in the dynamo context by Roberts (1972). The velocity field of the extended flow is given by

$$\boldsymbol{u} = \left(\frac{\partial \psi}{\partial y}, -\frac{\partial \psi}{\partial x}, K\psi\right), \tag{1.1a}$$

where K is a constant and

$$\psi = \sin x \sin y + \delta \cos x \cos y \quad (0 \leqslant \delta \leqslant 1). \tag{1.1b}$$

A few remarks on the terminology and the geometry of the flow (1.1) are in order. We shall refer to the (x, y)-plane as horizontal and the z-direction as vertical. The stream function (1.1b) defines a one-parameter, δ, family of steady flows independent of the vertical coordinate z. The Roberts (1972) flow corresponds to $\delta = 0$. Motion is confined to streamsurfaces ψ = constant and consequently the streamline topology is not influenced by the second parameter K, which plays a passive role in our theory. (In the kinematic dynamo problem, it will be important that $K \neq 0$, for only in this case is the alpha-effect non-zero. In the analysis of scalar transport, the z-component of (1.1a) will play no role.) For the special case $K = \sqrt{2}$, the motion (1.1) is the integrable case of the Beltrami flows considered by Dombre *et al.* (1986), obtained by setting one of the coefficients A, B, C equal to zero. The case $\delta = 0$ defines the square-cell flow with plane boundaries $\psi = 0$. A typical example of the case δ non-zero is illustrated in figure 1, which shows for $\delta = 0.3$ the streamsurfaces ψ = constant projected onto the horizontal (x, y)-plane. When $\delta > 0$, the cellular motion is confined to the cat's eyes, where $\delta \leqslant |\psi| \leqslant 1$. The separatrices, which bound these cat's eyes, intersect at the points $(x, y) = (m\pi, n\pi)$ for integer m, n, and are identified by the streamsurfaces $\psi = (-1)^{m+n}\delta$. The intersections $(x, y) = (m\pi, n\pi)$ are stagnation points of the flow when $\delta = 0$, but in general they are *junction streamlines* upon which the vertical velocity is $(-1)^{m+n}K\delta$. Between the cat's eyes, where $|\psi| \leqslant \delta$, motion is confined to open channels. In each channel the horizontal motion has a mean part aligned with the vector $(1, 1)$ but alternating in sign from one channel to the next. As δ increases the size of the cat's eyes decreases. The directional property of the mean channel flow is clearly seen in the limit $\delta \to 1$. In that limit the eyes disappear and the remaining flow is unidirectional with motion defined by the stream function $\psi = \cos(y - x)$. As we shall see, the symmetry about the direction

$$\boldsymbol{i}^{(+)} = (1, 1) \tag{1.2a}$$

and the mutually orthogonal direction

$$\boldsymbol{i}^{(-)} = (1, -1) \tag{1.2b}$$

are central to our analysis. Also, anticipating interest in the 2×2 diffusion and alpha-matrices, $\boldsymbol{D}$ and $\boldsymbol{\alpha}$ (see (1.8) and (1.20) below), we introduce the dyadics

$$\boldsymbol{I}^{(\pm)} = \tfrac{1}{2}\boldsymbol{i}^{(\pm)}\boldsymbol{i}^{(\pm)} = \frac{1}{2}\begin{bmatrix} 1 & \pm 1 \\ \pm 1 & 1 \end{bmatrix} \tag{1.2c}$$

defined by them.

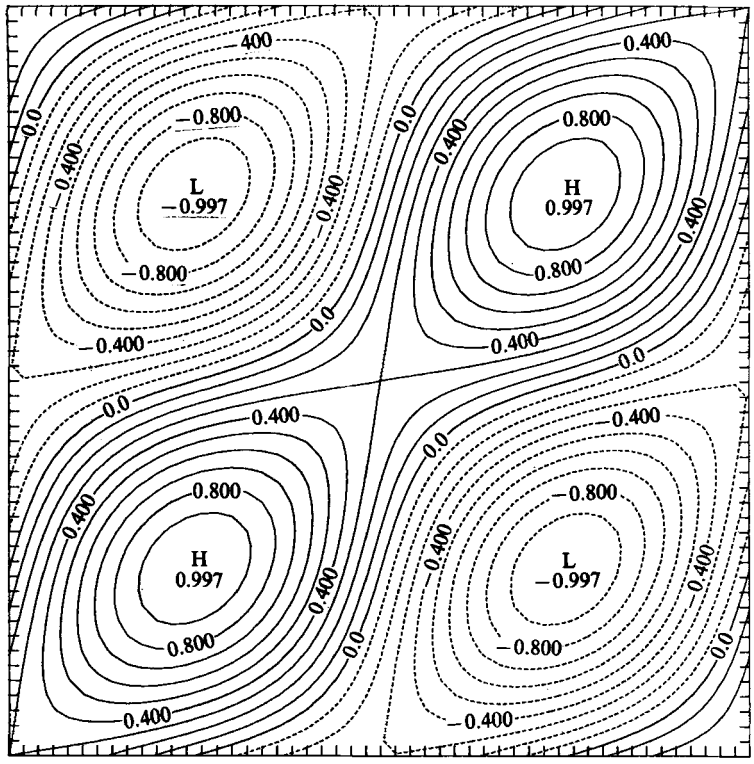

FIGURE 1. Streamlines of the flow (1.1) for $\delta = 0.3$. The channel is bounded by the streamlines $\psi = \pm 0.3$.

As already indicated, two distinct physical problems will be discussed in the paper. The main problem, which derives from the kinematic dynamo (Moffatt 1978; Zel'dovich, Ruzmaikin & Sokolov 1981), provided the original motivation for the work described here. This *magnetic* problem is, in our asymptotic theory, reduced to the study of two heat conduction equations (1.3) and (1.14) below, involving two scalars A and B. Fortunately these two equations can be solved successively, in two stages. The first stage consists of solving the homogeneous heat conduction equation (1.3) when there is a prescribed mean gradient of A. This is the *thermal* problem, in which A is used for temperature. It constitutes a well-defined and important problem in its own right, which introduces concisely the classical problem of bulk transport of a passive scalar. We regard the thermal problem as the core mathematical problem in this paper and shall frequently use its intuitive terminology in our discussion. So, for example, contours of constant A define isotherms in the thermal problem but define the horizontal projection of field lines in the magnetic problem, since A is the magnetic potential for the horizontal field. In particular, this means that the prescribed mean temperature gradient $\boldsymbol{g}_{\mathrm{H}}$ (see (1.4)) defines a uniform magnetic field $\bar{\boldsymbol{B}}_{\mathrm{H}}$ (see (1.12)) perpendicular to it.

The solution of the thermal problem is outlined in §1.2. It is a prerequisite for, and provides the first stage of, the complete solution of the magnetic problem outlined in §1.3. The second stage consists of solving the inhomogeneous heat conduction equation (1.14), in which the heat source on the right of the equation depends linearly on A. In both the thermal and magnetic problems only the case of large Reynolds number will be addressed in detail. The appropriate asymptotics is

outlined in §1.4. There are minor differences in the key matrices $\boldsymbol{D}$ (see (1.8)) and $\boldsymbol{\alpha}$ (see (1.20)) which emerge because $\boldsymbol{g}_{\mathrm{H}}$ is perpendicular to $\bar{\boldsymbol{B}}_{\mathrm{H}}$ and because B is absent in the thermal problem. Thus the reader interested only in the thermal problem can omit all subsequent Sections concerned with the calculation of B. The asymptotic evaluation of the coefficients of the diffusion matrix $\boldsymbol{D}$ and their tabular data are given in Appendix B.

1.2. *The thermal diffusion problem*

The *thermal* problem considers the advection–diffusion of a steady, z-independent, scalar temperature field $A(x, y)$ which satisfies the heat conduction equations

$$\boldsymbol{u}_{\mathrm{H}} \cdot \nabla A - \frac{1}{R} \nabla_{\mathrm{H}}^2 A = 0 \tag{1.3}$$

for a prescribed mean temperature gradient

$$(g_x, g_y) \equiv \boldsymbol{g}_{\mathrm{H}} = \overline{\nabla A}, \tag{1.4}$$

where the bar indicates a horizontal average. In (1.3), $\boldsymbol{u}_{\mathrm{H}} = (\partial\psi/\partial y, -\partial\psi/\partial x)$ is the horizontal velocity field, where the streamfunction ψ is given by (1.1*b*), and $R = UL/\kappa$ is the Péclet number; U is a reference velocity, $2\pi L$ is the period in x and y of the flow, and κ is the thermal diffusivity. The solution of the problem posed by (1.3) and (1.4) has the form,

$$A = \boldsymbol{g}_{\mathrm{H}} \cdot [\boldsymbol{x} + \boldsymbol{A}'(x, y)] + \text{constant}. \tag{1.5a}$$

Here the vector $\boldsymbol{A}'$ is independent of $\boldsymbol{g}_{\mathrm{H}}$, has zero horizontal average ($\overline{\boldsymbol{A}'} = 0$), and is defined by

$$2\boldsymbol{A}' = -\boldsymbol{i}^{(-)} A^{(+)}(x, y) + \boldsymbol{i}^{(+)} A^{(-)}(x, y), \tag{1.5b}$$

where $\boldsymbol{i}^{(\pm)}$ are given by (1.2*a*, *b*) and $A^{(\pm)}$ are the periodic solutions of

$$\frac{\partial(A^{(\pm)}, \psi)}{\partial(x, y)} - \frac{1}{R} \nabla^2 A^{(\pm)} = (1 \mp \delta) \sin(y \pm x). \tag{1.5c}$$

The quantity of physical interest derived from the solution is the mean heat flux

$$\boldsymbol{F}_{\mathrm{H}} \equiv \overline{\boldsymbol{u}_{\mathrm{H}} A} = (-\overline{\psi A_y}, \overline{\psi A_x}). \tag{1.6}$$

This result follows after an integration by parts which uses the fact that $\overline{\nabla(\psi A)}$ vanishes. We note also that (1.6) continues to hold when A is replaced by $\boldsymbol{g}_{\mathrm{H}} \cdot \boldsymbol{A}'$ (because $\overline{\psi \nabla \boldsymbol{A}} = \bar{\psi} \boldsymbol{g}_{\mathrm{H}} = 0$). Since the solution (1.5*a*) depends linearly on $\boldsymbol{g}_{\mathrm{H}}$, it follows that $\boldsymbol{F}_{\mathrm{H}}$ is linearly related to $\boldsymbol{g}_{\mathrm{H}}$ through a matrix $\boldsymbol{D}$. The symmetry properties of $\boldsymbol{D}$, which we will now determine, depend on the symmetry of the solutions $A^{(\pm)}$ of (1.5*c*).

We begin by identifying the two transformations which leave ψ and $\nabla(\boldsymbol{g}_{\mathrm{H}} \cdot \boldsymbol{A}')$ invariant. They are $(x, y) \to (x + m\pi, y + n\pi)$, where m, n are integers with even sum, and $(x, y) \to (-x, -y)$. The former is obvious and the latter depends upon the property $\boldsymbol{A}'(-x, -y) = -\boldsymbol{A}'(x, y)$. Each cat's eye is contained in square domains $D_{m,n} \equiv [m\pi, (m+1)\pi] \times [n\pi, (n+1)\pi]$, where m, n are arbitrary integers. The two neighbouring cat's eyes in $D_{0,0}$ and $D_{1,0}$ bound a channel $|\psi| \leqslant \delta$, which we refer to as the *primary* channel. In figure 1 the primary channel enters the square $[0, 2\pi] \times [0, 2\pi]$ on the lower boundary, and leaves on the right-hand boundary. Figure 2 (*a*) is obtained by a shift down by π, and shows the square $[0, 2\pi] \times [-\pi, \pi]$, so the primary channel crosses the side $O: (0, 0), P': (\pi, 0)$ of $D_{0,0}$ and the side $P: (\pi, \pi), P'': (2\pi, \pi)$ of $D_{1,0}$. The

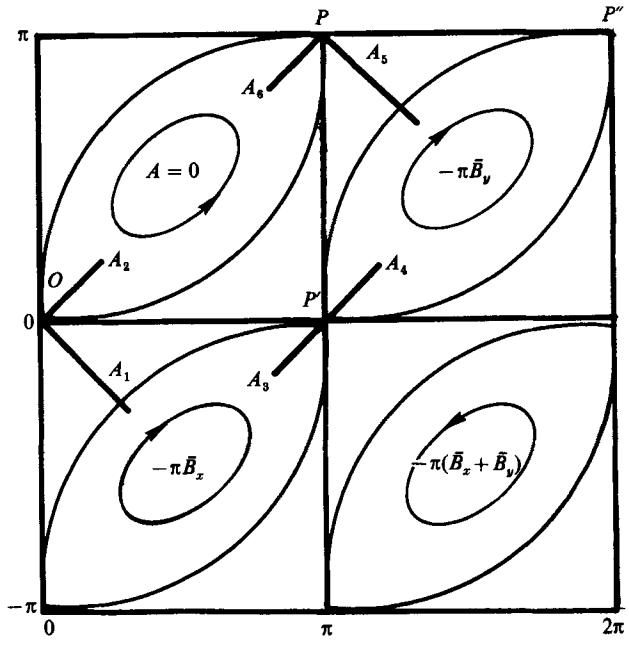

(*a*)

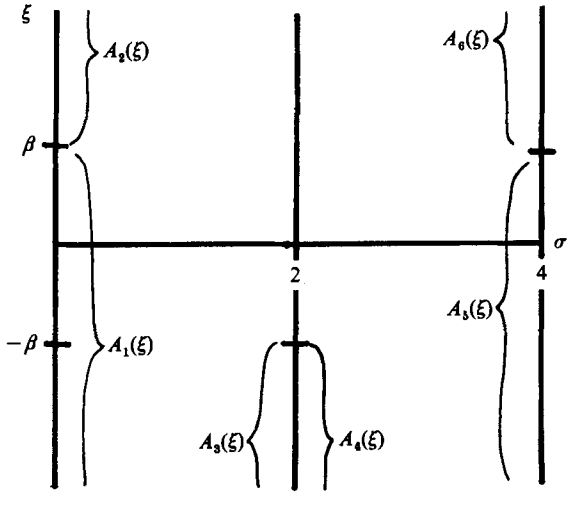

(*b*)

FIGURE 2. (*a*) The primary channel in the boundary-layer limit for the case $\bar{\boldsymbol{B}}_{\mathrm{H}} = (\bar{B}_x, \bar{B}_y)$, showing where various field profiles are defined relative to the streamlines bounding the cat's eyes. (*b*) The boundary-layer problem in (σ, ξ)-coordinates.

parallelogram $OP'P''P$ can be mapped by the two transformations into the entire (x, y)-plane. Since the mappings leave $\psi \nabla A'$ invariant, the parallelogram thus defines the smallest region over which we may take the horizontal average (1.6). In practice, we find it more convenient (because of the geometry of the boundary layers, cf. §2) to take averages over the rectangle D_0 of area π^2 with corners at $(0, 0), (\frac{1}{2}\pi, -\frac{1}{2}\pi)$,

$(\frac{3}{2}\pi, \frac{1}{2}\pi), (\pi, \pi)$. The boundary of D_0 is indicated by the lines A_{1-6} in figure 2(*a*). (The lines also indicate where boundary-layer profiles are to be evaluated, in §2.)

Additional symmetries can be identified from the transformation $(x, y) \to (y+\pi, x)$, which again maps $D_{0,0}$ onto $D_{1,0}$. (Note, in particular, the interchange of x and y.) By this latter transformation, ψ changes sign, while the solutions $A^{(\pm)}$ of (1.5*c*) have the property $-A^{(\pm)}(y+\pi, x) = \pm A^{(\pm)}(x, y)$. Accordingly we have the important result

$$\overline{\psi\, \partial A^{(\pm)}/\partial x} = \pm \overline{\psi\, \partial A^{(\pm)}/\partial y} = -D^{(\pm)}, \tag{1.7}$$

say, which relates the two components of F_x and F_y of the mean heat flux (1.6). By (1.5*b*) the relations are

$$\boldsymbol{i}^{(+)} \cdot (\boldsymbol{F}_{\mathrm{H}} + D^{(-)} \boldsymbol{g}_{\mathrm{H}}) = 0, \quad \boldsymbol{i}^{(-)} \cdot (\boldsymbol{F}_{\mathrm{H}} + D^{(+)} \boldsymbol{g}_{\mathrm{H}}) = 0, \tag{1.8a}$$

from which we deduce that

$$\boldsymbol{F}_{\mathrm{H}} = -\boldsymbol{D} \cdot \boldsymbol{g}_{\mathrm{H}}. \tag{1.8b}$$

Here $\boldsymbol{D}$ is the matrix

$$\boldsymbol{D} = D^{(+)} \boldsymbol{I}^{(-)} + D^{(-)} \boldsymbol{I}^{(+)}, \tag{1.8c}$$

where $\boldsymbol{I}^{(\pm)}$ are the dyadics (1.2*c*).

The result (1.8) of our idealized problem has important physical implications. If, for example, the mean gradient $\boldsymbol{g}_{\mathrm{H}}$ (and possibly also the cellular motion itself) vary on a lengthscale large compared with the cell size L, then the equation for the mean temperature would involve the divergence of the mean heat flux $\boldsymbol{F}_{\mathrm{H}}$. This leads to the well-known idea of an eddy diffusivity for which the total diffusion of the mean temperature $\bar{A}$ is governed by the divergence of the effective Fickian heat flux

$$-\boldsymbol{D}_{\mathrm{eff}} \cdot \boldsymbol{g}_{\mathrm{H}}, \tag{1.9a}$$

where

$$\boldsymbol{D}_{\mathrm{eff}} = \boldsymbol{D} + \frac{1}{R} \boldsymbol{I}. \tag{1.9b}$$

Our problem is to determine the eigenvalues $D^{(\pm)}$ of the matrix $\boldsymbol{D}$ as functions of R.

1.3. *The kinematic dynamo problem*

The *magnetic* problem considers the advection–diffusion of a steady, z-independent, vector magnetic field $\boldsymbol{B}(x, y)$ which satisfies the magnetic induction equations

$$\boldsymbol{\nabla} \times (\boldsymbol{u} \times \boldsymbol{B}) + \frac{1}{R} \nabla^2 \boldsymbol{B} = 0 \quad (\boldsymbol{\nabla} \cdot \boldsymbol{B} = 0), \tag{1.10}$$

where $R = UL/\eta$ is now the magnetic Reynolds number of the flow based upon the magnetic diffusivity η of the now electrically conducting fluid. The magnetic field is given by

$$\boldsymbol{B}(x, y) = (B_x, B_y, B_z) = \left(\frac{\partial A}{\partial y}, -\frac{\partial A}{\partial x}, KB \right). \tag{1.11}$$

where the vertical component has been scaled with factor K present in the vertical component of velocity (see (1.1*a*)). The horizontal components of (1.10) imply that the magnetic potential A, which defines the horizontal magnetic field $\boldsymbol{B}_{\mathrm{H}}$, satisfies the heat conduction equation (1.3). This equation is to be solved subject to the condition that the mean horizontal magnetic field is prescribed:

$$(\bar{B}_x, \bar{B}_y) = (\overline{\partial A/\partial y}, -\overline{\partial A/\partial x}) = (g_y, -g_x). \tag{1.12}$$

The mathematical problem which emerges is identical to that outlined by (1.5). The two distinct solutions $A^{(+)}$ and $A^{(-)}$ now correspond to the mean horizontal fields

$$\bar{\boldsymbol{B}}_{\mathrm{H}} = \boldsymbol{i}^{(+)} \quad \text{and} \quad \boldsymbol{i}^{(-)} \tag{1.13}$$

(see (1.2)), which are directed parallel and perpendicular to the symmetry direction (1, 1) isolated in §1.1.

The vertical component of (1.10), on the other hand, implies that B is governed by the inhomogeneous heat conduction equation

$$\boldsymbol{u}_{\mathrm{H}}\cdot\nabla B-\frac{1}{R}\nabla_{\mathrm{H}}^2 B=-\boldsymbol{u}_{\mathrm{H}}\cdot\nabla A, \tag{1.14}$$

in which the term on the right supplies a source of heat. This equation is to be solved subject to the boundary condition that there is no mean vertical magnetic field

$$\bar{B}=0. \tag{1.15}$$

The solutions of (1.14) have a form similar to (1.5) and are given by

$$B=\bar{\boldsymbol{B}}_{\mathrm{H}}\cdot\boldsymbol{B}', \tag{1.16a}$$

where

$$2\boldsymbol{B}'=\boldsymbol{i}^{(+)}B^{(+)}(x,y)+\boldsymbol{i}^{(-)}B^{(-)}(x,y) \tag{1.16b}$$

and we recall that

$$\boldsymbol{i}^{(+)}\cdot\bar{\boldsymbol{B}}_{\mathrm{H}}=-\boldsymbol{i}^{(-)}\cdot\boldsymbol{g}_{\mathrm{H}},\quad \boldsymbol{i}^{(-)}\cdot\bar{\boldsymbol{B}}_{\mathrm{H}}=\boldsymbol{i}^{(+)}\cdot\boldsymbol{g}_{\mathrm{H}}. \tag{1.16c}$$

The two spatially periodic functions $B^{(\pm)}$ are solutions of

$$\frac{\partial(B^{(\pm)},\psi)}{\partial(x,y)}-\frac{1}{R}\nabla^2 B^{(\pm)}=\frac{\partial(\psi,A^{(\pm)})}{\partial(x,y)}+(1\mp\delta)\sin(y\pm x), \tag{1.16d}$$

and have the same symmetries as $A^{(\pm)}$.

The quantity of physical interest is the mean electromotive force $\overline{\boldsymbol{u}\times\boldsymbol{B}}$. The vertical component is

$$-\overline{\nabla\cdot(\boldsymbol{u}_{\mathrm{H}}A)}=-\nabla\cdot\boldsymbol{F}_{\mathrm{H}} \tag{1.17}$$

(see (1.6)), which vanishes because $\boldsymbol{F}_{\mathrm{H}}$ is a constant vector. The remaining horizontal components will be denoted by $K\bar{\boldsymbol{E}}_{\mathrm{H}}$ and are given by

$$K\bar{\boldsymbol{E}}_{\mathrm{H}}\equiv\overline{\boldsymbol{u}\times\boldsymbol{B}}=K\overline{(\psi\nabla A-B\nabla\psi)}. \tag{1.18}$$

Since $\overline{\psi\nabla A}$ is linked to $\boldsymbol{F}_{\mathrm{H}}$ by (1.6), and in view of the symmetries of B, it is a simple matter to establish the result

$$\overline{(\psi\,\partial A^{(\pm)}/\partial x-\partial\psi/\partial x B^{(\pm)})}=\pm\overline{(\psi\,\partial A^{(\pm)}/\partial y-\partial\psi/\partial y B^{(\pm)})}=-\alpha^{(\pm)}, \tag{1.19}$$

say. It follows, as in (1.8) above, that

$$K\bar{\boldsymbol{E}}_{\mathrm{H}}=\boldsymbol{\alpha}\cdot\bar{\boldsymbol{B}}_{\mathrm{H}} \tag{1.20a}$$

where

$$-K^{-1}\boldsymbol{\alpha}=\alpha^{(+)}\boldsymbol{I}^{(+)}+\alpha^{(-)}\boldsymbol{I}^{(-)}. \tag{1.20b}$$

The x- and y-components of (1.20a) are given by

$$\bar{E}_x=\tfrac{1}{2}\bar{\boldsymbol{B}}_{\mathrm{H}}\cdot(\alpha^{(+)}\boldsymbol{i}^{(+)}+\alpha^{(-)}\boldsymbol{i}^{(-)})=\frac{1}{\pi^2}\iint_{D_0}\left(\psi\frac{\partial A}{\partial x}-\frac{\partial\psi}{\partial x}B\right)\mathrm{d}x\,\mathrm{d}y, \tag{1.21a}$$

$$\bar{E}_y=\tfrac{1}{2}\bar{\boldsymbol{B}}_{\mathrm{H}}\cdot(\alpha^{(+)}\boldsymbol{i}^{(+)}-\alpha^{(-)}\boldsymbol{i}^{(-)})=\frac{1}{\pi^2}\iint_{D_0}\left(\psi\frac{\partial A}{\partial y}-\frac{\partial\psi}{\partial y}B\right)\mathrm{d}x\,\mathrm{d}y, \tag{1.21b}$$

where the rectangle D_0, of area π^2, was introduced and defined in §1.2 above.

As in the case of the *thermal* problem described in the previous Subsection, the mean electromagnetic force (1.20) which we seek to evaluate is important when mean fields are allowed to vary on a scale large compared with the flow. Then the induced

current can be computed locally and used to construct a much simpler dynamo problem on the larger scale leading, for example, to the so-called α^2-dynamos (cf. Moffatt 1978). Here we are concerned only with the local problem in which the mean field is taken as horizontal and constant. It should be remarked, however, that the growth rate of the α^2-dynamo depends on the determinant of the alpha-matrix (see (5.1) below), which is simply the product of its eigenvalues:

$$\det(\boldsymbol{\alpha}) = K^2\alpha^{(+)}\alpha^{(-)}. \tag{1.22}$$

For the dynamo to operate it is necessary that the determinant, and therefore both eigenvalues, be non-zero.

1.4. *Asymptotics for large R*

The most important assumption that we shall make is that the parameter R appearing in (1.3) and (1.14) is very large:

$$R \gg 1. \tag{1.23}$$

Childress (1979, hereafter denoted by C) treated the above magnetic problem for the Roberts' flow given by (1.1) with $\delta = 0$, with the assumption (1.23). The boundary-layer methods used there also apply to the case $\delta > 0$, but the geometry of the boundary layers is different owing to the presence of the channels. The regions of closed streamlines within the eyes in figure 1 are regions of 'flux expulsion' where, for $R \gg 1$, the scalar fields A and B are well mixed and therefore approach constants. The process of flux expulsion will not be discussed here but a recent discussion has been given by Rhines & Young (1983). The separatrices of the cat's eyes thus locate the boundary layers of thickness order $R^{-\frac{1}{2}}$, and it is clear that the parameter that measures the ratio of channel to boundary-layer width is

$$\beta \equiv \delta R^{\frac{1}{2}}. \tag{1.24}$$

When β is of order unity, the boundary layers on either side of a given channel are superimposed and must be treated as one structure. If β is large the channels divide the magnetic layers on either side and the latter can be treated as distinct boundary-layer structures, which match at their outer edges with the flow in the eyes and channels. When $\beta \gg 1$, we thus can split up the problem into outer or 'mainstream' solutions, and inner or boundary-layer solutions, the key step being to effect a proper matching of the two. This leads us to adopt the following organization of the paper. In §2 we present the boundary-layer problem formulated for numerical computation at fixed β. We there explore the overall structure of the solution and the dependence of observables on β. Sections 3 and 4 attempt an analytic approach to the dual limit of large R and large β, needed to discuss the limit of large R at fixed δ. The mainstream analysis of §3 utilizes Prandtl–Batchelor (1904, 1956) theory to obtain the limiting forms of the fields within the channels and eyes, up to boundary-layer corrections. These mainstream solutions provide the edge conditions (zeroth-order matching conditions) needed to determine the structure of individual (non-interacting) boundary layers, and this analysis, which utilizes the Wiener–Hopf technique, is summarized in §4. Some of the details concerning these analytic solutions, which have application to other advection–diffusion problems (see, for example, Brown & Stewartson 1978), are collected in Appendix A.

Insofar as the computation of $\boldsymbol{\alpha}$ is concerned, the case $\delta = 0$, first studied for arbitrary R by Roberts (1972), exhibits an additional symmetry under the reflection $(x, y) \to (-x, y)$, namely $A^{(+)}(x, y) = A^{(-)}(-x, y)$ and $B^{(+)}(x, y) = B^{(-)}(-x, y)$. By (1.7)

and (1.19) these relations imply that $D^{(+)} = D^{(-)} = D$, say, and $\alpha^{(+)} = \alpha^{(-)} = \alpha$, say. Therefore, the resulting diffusion and alpha-matrices are isotropic,

$$\boldsymbol{D} = D\boldsymbol{I}, \quad \boldsymbol{\alpha} = -K\alpha\boldsymbol{I}, \quad (\boldsymbol{I}^{(+)} + \boldsymbol{I}^{(-)} = \boldsymbol{I}). \tag{1.25a}$$

The asymptotic analysis in C shows that, correct to lowest order,

$$\tfrac{1}{2}D = \alpha = R^{-\frac{1}{2}}\alpha_0 \quad (\alpha_0 = 0.5327\ldots) \tag{1.25b}$$

(see also Appendix B). The value of α_0, which was estimated approximately in C, was addressed by the numerical studies of Anufriyev & Fishman (1982), and Perkins & Zweibel (1987), while its analytic evaluation was given by Soward (1987), hereafter denoted by S; see also Soward (1989).

At the other extreme, $\delta = 1$, for which the cat's eyes disappear and $\psi = \cos(y-x)$, there is no mean induction when the mean magnetic field is aligned with the unidirectional horizontal motion (i.e. $\bar{\boldsymbol{B}}_{\mathrm{H}} = \boldsymbol{i}^{(+)}$, see (1.13)). Indeed exact solutions of (1.5*c*) and (1.16*d*) are readily obtained. They are

$$A^{(+)} = B^{(+)} = 0, \quad A^{(-)} = B^{(-)} = R\sin(y-x). \tag{1.26a, b}$$

From (1.7) and (1.19) we see that the eigenvalues $D^{(+)}$ and $\alpha^{(+)}$ vanish, leaving

$$\boldsymbol{D} = \tfrac{1}{2}R\boldsymbol{I}^{(+)}, \quad \boldsymbol{\alpha} = -KR\boldsymbol{I}^{(-)}. \tag{1.27a, b}$$

The last result has important implications for the dynamo problem. We have already indicated below (1.22) that the dynamo will not operate when $\alpha^{(+)}$ vanishes and so the case $\delta = 1$ is not a dynamo. The results given below show that, for large R, the coefficient $\alpha^{(+)}$ tends to zero quickly with increasing δ. The actual values of $\alpha^{(+)}$ and $\alpha^{(-)}$ are computed numerically from equations derived by boundary-layer theory for various values of β (see table 1). Analytic expressions for them are obtained when β is large, but still restricted to the case of narrow channels ($\delta \ll 1$). At leading order they are

$$\alpha^{(-)} = O(R\delta^3), \quad \alpha^{(+)} = O(R^{-\frac{3}{2}}\delta^{-2}) \quad (R^{-\frac{1}{2}} \ll \delta \ll 1) \tag{1.28a, b}$$

(see (3.23), (3.24)). The former large result for $\alpha^{(-)}$ is determined with relative ease from the mainstream solution of §3. The latter small result for $\alpha^{(+)}$ emerges from boundary-layer corrections to the mainstream solution. The asymptotic behaviour of $\alpha^{(+)}$ provided the stimulus for the detailed Wiener–Hopf calculation used to solve the boundary-layer problem. The results show that, despite the fact that $\alpha^{(+)}$ tends to zero with increasing δ, the key quantity $\det(\boldsymbol{\alpha})$ actually increases linearly with δ; in this sense we conclude that the channels enhance the alpha-effect. As the results (1.28) indicate, the analysis of the boundary-layer structure is an essential ingredient in deciding the basic question of dynamo activity.

The estimate of the alpha-effect for large R leads naturally to the question of 'fast' dynamo action, that is, the presence of dynamo activity in the limit of infinite R. This question is addressed for our two-dimensional flows by seeking solutions with the mean magnetic field $\bar{\boldsymbol{B}}_{\mathrm{H}}$ proportional to $\mathrm{e}^{pt+\mathrm{i}nz}$, where p is the growth rate and n is the wavenumber in z. When $\delta = 0$, (1.25) and (5.1) below show that the growth rate at fixed n is proportional to $KR^{-\frac{1}{2}}\alpha_0 n$ as $R \to \infty$. This result suggests that fast dynamo activity is possible when n is of order $R^{\frac{1}{2}}$, corresponding to vertical lengthscales comparable with the boundary-layer thickness $R^{-\frac{1}{2}}$. The case $\delta = 0$ was considered in S, where it was shown that in the limit $R \to \infty$ the growth rate is $KR^{-\frac{1}{2}}\nu n$, where now $\nu(\mu)$ is a function of $\mu = R^{-\frac{1}{2}}(\ln R)\,n$ and $\nu(0) = \alpha_0$. Recently Galloway & Frisch (1986) have, like Roberts (1972) before, employed modal expansions and solved the magnetic induction equation directly for R ranging up to values in excess of 10^3,

without making the boundary-layer approximations used in the present paper. Soward (1989) has shown that their results confirm the dependence of ν upon μ predicted by the asymptotic theory. One point which emerges from these investigations is that the underlying dynamo process for μ of order unity is adequately described by the theory of C for $\mu = 0$. There are, of course, quantitative differences, but the central issues are isolated by the case $\mu = 0$. In this paper we shall not address the question of the dependence of the alpha-matrix on μ, and so the work provides the extension to $\delta > 0$ of C but not of S. For additional discussion of the implications of our results with $\mu = 0$, for dynamo action on vertical lengthscales of order δ, see §5.

Before proceeding we comment briefly upon our choice of velocity (1.1). Dynamo action at large R is sensitive to the location of the boundary layers, and for three-dimensional flows, such as the Beltrami ABC flow, they may become very complicated. Galloway & Frisch (1986) have presented pertinent numerical results for large R. Some analytic progress has been made (see C, and Childress & Soward 1985) but no robust theory is yet available. The aim in this paper is to break the symmetry of the Roberts motion ($\delta = 0$) in a relatively simple way to determine the effect on the inductive processes. The relative simplicity of (1.1) with $\delta > 0$ is a result of the geometry of the streamlines. These are either closed within the cat's eyes or infinite-periodic in the channels. A fluid particle thus has a simple trajectory in either case. By adjusting the parameters of the ABC flow, more complicated structure may be obtained, including regions of Lagrangian chaos. Consequently the present results comprise a first step in the breaking of the symmetry of the Roberts motion, which could in principle extend to flows which have some of the features thought to favour fast dynamo action. Insofar as (1.1) is concerned, the fast dynamo issue is of interest, but it will not be the main concern of the present study.

2. The boundary-limit layer

The present Section is devoted to the formulation and solution of the boundary-layer problem which determines scalar transport and alpha-effect at large R when β, as defined by (1.24), is of order unity. The notation and general procedure is similar to that of S and C, but is complicated by the opening of the channels for positive β.

2.1. *Formulation*

When δ is small the section of the *primary* channel $|\psi| < \delta$, identified in § 1.2 and lying within the averaging rectangle D_0, is close to the two straight line segments OP' and $P'P$ illustrated in figure 2(*a*) while the cat's eyes almost fill the squares $D_{m,n}$. When the channel and magnetic boundary-layer widths are comparable (i.e. $\beta = O(1)$, cf. (1.24)), the boundary-layer analysis closely follows the $\delta = 0$ case. Indeed the boundary-layer equations for A and B are the same as for that case, namely

$$\frac{\partial A}{\partial \sigma} - \frac{\partial^2 A}{\partial \xi^2} \equiv H[A] = 0, \quad H[B] = -\frac{\partial A}{\partial \sigma}, \tag{2.1 a, b}$$

where, if $q = |\boldsymbol{u}|$ and s measures arclength,

$$\sigma = \int_0^s q \, \mathrm{d}s, \quad \xi = R^{\frac{1}{2}}\psi. \tag{2.1 c, d}$$

Thus σ is circulation along the boundary layer, while ξ is a stretched stream function.

Since magnetic flux is expelled from the cat's eyes (cf. §3.2 below), the values of A and B are constant in the eyes, and for the mean field (1.12) the appropriate constants are

$$A^{\mathrm{MS}} = \pi(n\bar{B}_x - m\bar{B}_y), \quad B^{\mathrm{MS}} = 0 \text{ on } D_{m,n}, \tag{2.2a, b}$$

where m, n are arbitrary integers, and the constant in (1.5a) has been given the value $-(\pi/2)\,\boldsymbol{i}^{(-)}\cdot\bar{\boldsymbol{B}}_{\mathrm{H}}$. The solutions of (2.1) must, therefore, satisfy the boundary conditions

$$A \to A^{\mathrm{MS}}, \quad B \to 0 \quad \text{as} \quad |\xi| \to \infty. \tag{2.3a, b}$$

When we consider the primary channel it is natural to measure arclength s from the origin O (see figure 2a). Fluid flows from O to P', where $\sigma = 2$, and on to P, where $\sigma = 4$. The channel is bounded from above by the streamline $\xi = \beta$, which bounds the cat's eye $D_{0,0}$ between O and P, and below by the streamline $\xi = -\beta$, which passes through P', and bounds the cat's eyes $D_{0,-1}$ (on $0 < \sigma < 2$) and $D_{1,0}$ (on $2 < \sigma < 4$).

In figure 2(a) we also sketch the various positions where profiles of A and B will be evaluated. The boundary-layer theory amounts to following the fields as they develop, down the primary channel say, and then using the symmetry of the flow and the secular variation of A arising from the mean field to derive relations between the profiles at distinct points along the channel. The profiles can be related as the boundary layer passes near to the X-type neutral points where the separatrices cross. We refer to these points as 'corners' since the boundary layers are turned at the corners and a natural matching of profiles is established. The asymptotics of the corner matching is discussed in C, and by Anufriyev & Fishman (1982). From (2.1a) we see that profiles of A evolve as solutions of a homogeneous one-dimensional heat equation, the mainstream values (2.3a) providing the boundary conditions. Related procedures apply for the inhomogeneous equation (2.1b) with homogeneous boundary condition (2.3b).

To be more precise, we define the profiles shown in figure 2(a) by

$$A(0_+, \xi) = \begin{cases} A_2(\xi), & (\xi > \beta), \\ A_1(\xi), & (\xi < \beta), \end{cases} \tag{2.4a}$$

$$A(4_-, \xi) = \begin{cases} A_6(\xi), & (\xi > \beta), \\ A_5(\xi), & (\xi < \beta), \end{cases} \tag{2.4b}$$

$$A(2_+, \xi) = A_4(\xi), \quad A(2_-, \xi) = A_3(\xi) \quad (\xi < -\beta), \tag{2.4c}$$

where the subscripts $+$ and $-$ are used to indicate whether the value of σ referred to is approached from above or below. The corresponding locations in the (σ, ξ)-plane are shown in figure 2(b). The corner regions in figure 2(a) mark the location of the transition region where matching of the boundary-layer profiles occurs. The spatial periodicity together with the secular increase of A down the channels implies that

$$A_1 + \pi\bar{B}_x = A_5 + \pi\bar{B}_y. \tag{2.5a}$$

The symmetry of the flow and A about the diagonal OP of the cat's eye $D_{0,0}$ implies (the mainstream value in this primary cell being zero) that

$$A_2 = -A_6. \tag{2.5b}$$

The value A_7 at the corner $P'' : (2\pi, \pi)$ may be derived from A_3 by the secularity argument or from A_4 by the symmetry argument. Together they yield

$$A_3 + \pi\bar{B}_x [= A_7 + \pi\bar{B}_y] = -(A_4 + \pi\bar{B}_y). \tag{2.5c}$$

An important observation concerns the regularity of the field profiles as the continuation described above is carried out. Since the initial-value problem for the heat equation produces analytic profiles downstream, we have, in particular, that all 'terminal' profiles entering a corner are analytic. However, portions of the profile within the eye and channel arrive at the corners from different regions, and therefore they need not agree on the separatrix, where A or B can be discontinuous. For example, the profiles A_1 and A_2 need not agree at O (see figure 2(*a*)). As a result boundary layers are 'triggered' at the corners from these discontinuities.

To avoid dealing with the additive constants in (2.5) it is actually more convenient to work with

$$b(\sigma, \xi) = \frac{\partial A}{\partial \xi}. \tag{2.6}$$

Since, as we have just seen, $A(0_+, \xi)$ and $A(2_+, \xi)$ are in general discontinuous at $\xi = \beta$ and $-\beta$ respectively, differentiation of A introduces heat sources Q_0 and Q_2 (see (2.8) below) at O and P' respectively. Their strength is determined so that the appropriate integral of b results (see (2.10) below). We therefore set

$$\begin{bmatrix} f_{A0}(\xi) \\ f_{A2}(\xi) \end{bmatrix} = \begin{bmatrix} b(2_-, \xi) \\ b(4_-, \xi) \end{bmatrix}, \quad \begin{bmatrix} g_{A0}(\xi) \\ g_{A2}(\xi) \end{bmatrix} = \begin{bmatrix} b(0_+, \xi) \\ b(2_+, \xi) \end{bmatrix}_{\text{reg}}, \tag{2.7}$$

where in the latter case the regular part of the functions is taken on the right. Then, in terms of the initial values at $\sigma = 0$ and 2, the Green-function solutions of (2.1*a*) are

$$(4\pi\sigma)^{\frac{1}{2}} b(\sigma, \xi) = Q_0 \, \mathrm{e}^{-(\xi-\beta)^2/4\sigma} + \int_{-\infty}^{+\infty} g_{A0}(u) \, \mathrm{e}^{-(\xi-u)^2/4\sigma} \, \mathrm{d}u, \tag{2.8a}$$

$$(4\pi\sigma)^{\frac{1}{2}} b(\sigma+2, \xi) = Q_2 \, \mathrm{e}^{-(\xi+\beta)^2/4\sigma} + \int_{-\infty}^{+\infty} g_{A2}(u) \, \mathrm{e}^{-(\xi-u)^2/4\sigma} \, \mathrm{d}u \tag{2.8b}$$

on the sides OP' and $P'P$ respectively. The symmetry and periodicity conditions (2.5) imply that

$$g_{A0} = \operatorname{sgn}(\beta - \xi) f_{A2}(\xi), \quad g_{A2} = \operatorname{sgn}(\beta + \xi) f_{A0}(\xi), \tag{2.9}$$

while the boundary conditions (2.2) and (2.3) imply that

$$\int_{-\infty}^{+\infty} f_{A0}(\xi) \, \mathrm{d}\xi = \pi \bar{B}_x, \quad \int_{-\infty}^{+\infty} f_{A2}(\xi) \, \mathrm{d}\xi = \pi \bar{B}_y. \tag{2.10}$$

It is now convenient to consider separately the two cases of a magnetic field $\bar{\boldsymbol{B}}_{\mathrm{H}} = \boldsymbol{i}^{(+)}$ parallel to, and $\bar{\boldsymbol{B}}_{\mathrm{H}} = \boldsymbol{i}^{(-)}$ perpendicular to, the channels and cat's eyes (see (1.13)). The latter case, in which the mean magnetic field is transverse to the channel flow, is the more interesting because the mean magnetic field is susceptible to folding and stretching by the flow down the channel; a feature already exhibited by the solution (1.26) and (1.27). For these cases, (2.7)–(2.10) simplify giving

$$f_A \equiv f_{A0}(\xi) = \pm f_{A2}(-\xi), \quad g_A \equiv g_{A0}(\xi) = \pm g_{A2}(-\xi), \quad Q \equiv Q_0 = \pm Q_2, \tag{2.11a–c}$$

where

$$g_A(\xi) = \pm \operatorname{sgn}(\beta - \xi) f_A(-\xi), \quad \int_{-\infty}^{+\infty} f_A(\xi) \, \mathrm{d}\xi = \pi. \tag{2.12a, b}$$

Here and in the equations that follow the upper and lower signs correspond to $\bar{\boldsymbol{B}}_{\mathrm{H}} = \boldsymbol{i}^{(+)}$ (the parallel case) and $\bar{\boldsymbol{B}}_{\mathrm{H}} = \boldsymbol{i}^{(-)}$ (the perpendicular case) respectively. This procedure clearly identifies the appropriate case and so we drop the superscript

notation $(\pm)$ employed in §1, except where they are used to define the diffusion and alpha-matrix eigenvalues. When (2.8*a*, *b*) are evaluated with $\sigma = 2$, they lead with (2.11) and (2.12*a*) to the single integral equation

$$Q\,\mathrm{e}^{-(\xi-\beta)^2/8} \pm \int_{-\infty}^{+\infty} \mathrm{sgn}\,(\beta+u) f_A(u)\,\mathrm{e}^{-(\xi+u)^2/8}\,\mathrm{d}u = (8\pi)^{\frac{1}{2}} f_A(\xi), \tag{2.13a}$$

where, with the help of (2.12*b*), Q is fixed by

$$\pi = Q \pm \int_{-\infty}^{+\infty} \mathrm{sgn}\,(\beta+u) f_A(u)\,\mathrm{d}u. \tag{2.13b}$$

Once b is found we may solve for B by noting that it satisfies (2.1*b*) with a solution of the homogeneous heat equation on the right. We then select a particular solution which is well-behaved in that it avoids the heat sources on the initial line which are present in A. We are then free to add a solution of the heat equation, and make the sum of the two terms compatible with the boundary and initial conditions on B. Thus the solution of (2.1*b*) on the first section OP' of the primary channel is expressed in the form

$$B = \tfrac{1}{2}(\xi-\beta)\, b(\sigma,\xi) + C(\sigma,\xi) \quad (0 < \sigma < 2), \tag{2.14}$$

where C is a bounded homogeneous solution of the heat conduction equation (2.1*a*). On the second section $P'P$ of the channel, $(\xi-\beta)$ in (2.14) is replaced by $(\xi+\beta)$. Defining $f_{B,C}$ and $g_{B,C}$ as in (2.11*a*, *b*) by the values of B, C at $\sigma = 2_-$ and 0_+ respectively, we see from (2.14) that they are related by

$$g_B(\xi) = [\tfrac{1}{2}(\xi-\beta)]\, g_A(\xi) + g_C(\xi), \quad f_B(\xi) = [\tfrac{1}{2}(\xi-\beta)] f_A(\xi) + f_C(\xi). \tag{2.15a, b}$$

For the particular case of aligned and orthogonal mean magnetic fields, we note that B has the symmetry with respect to ξ of A and not $b\,(\equiv \partial A/\partial\xi)$. Consequently in place of (2.12*a*) we have

$$-g_B(\xi) = \pm\,\mathrm{sgn}\,(\beta-\xi) f_B(-\xi), \tag{2.16}$$

and in place of (2.13*a*) we have

$$\int_{-\infty}^{+\infty} g_C(u)\,\mathrm{e}^{-(\xi-u)^2/8}\,\mathrm{d}u = (8\pi)^{\frac{1}{2}} f_C(\xi). \tag{2.17}$$

From (2.12*a*), (2.15) and (2.16) we deduce that

$$-g_C(\xi) = \pm\,\mathrm{sgn}\,(\beta-\xi)\, h(-\xi), \tag{2.18a}$$

where

$$h(\xi) \equiv f_C(\xi) - \beta f_A(\xi). \tag{2.18b}$$

With (2.17) they lead to the integral equation

$$h(\xi) + \beta f_A(\xi) \pm (8\pi)^{-\frac{1}{2}} \int_{-\infty}^{+\infty} \mathrm{sgn}\,(\beta+u)\, h(u)\,\mathrm{e}^{-(\xi+u)^2/8}\,\mathrm{d}u = 0. \tag{2.19}$$

Finally, the alpha-matrix is calculated from (1.21). The contributions from the integrals (1.21*a*) and (1.21*b*) stem from the channel sections $P'P$ and OP' respectively. For our parallel and perpendicular fields, (1.21) (or equivalently (1.19)) gives

$$\pm R^{\frac{1}{2}} \alpha^{(\pm)} = \pm E_{P'P} = -E_{OP'}, \tag{2.20}$$

where

$$E = \frac{1}{\pi} \int_{-\infty}^{+\infty} (\xi b - B)\,\mathrm{d}\xi \tag{2.21}$$

			$R^{\frac{1}{2}}\alpha^{(+)}$		$R^{\frac{1}{2}}\alpha^{(-)}$		$K^{-2}R\det(\alpha)$	
β	N	L	Numerical	Asymptotic	Numerical	Asymptotic	Numerical	Asymptotic
0	97	24	0.5327	0.5180	0.5327	0.4090	0.2838	0.2119
0.5	103	25	0.2246	0.2248	1.383	1.320	0.3106	0.2967
1.0	101	24	0.1186	0.1250	3.377	3.455	0.4005	0.4319
1.5	107	25	0.07667	0.07941	7.203	7.314	0.5523	0.5808
2.0	105	24	0.05467	0.05489	13.37	13.40	0.7309	0.7355
2.5	111	25	0.04052	0.04019	22.25	22.20	0.9016	0.8922
3.0	109	24	0.03088	0.03070	34.28	34.24	1.059	1.051
3.5	115	25	0.02424	0.02421	50.01	49.99	1.212	1.210
4.0	113	24	0.01957	0.01958	69.96	69.97	1.369	1.370

TABLE 1. Summary of numerical and asymptotic solutions of the integral equations (2.13) and (2.19)

takes the constant values $E_{P'P}, E_{OP'}$ along the section indicated by the subscript. The constancy of E is readily established by showing that $\mathrm{d}E/\mathrm{d}\sigma$ vanishes, except possibly at corners. With $E_{OP'}$ evaluated at $P'(\sigma = 2)$ using (2.15b), (2.18) and (2.19) the result (2.20) becomes

$$\pm R^{\frac{1}{2}}\alpha^{(\pm)} = -\tfrac{1}{2}\beta - \frac{1}{\pi}\int_{-\infty}^{+\infty} [\tfrac{1}{2}uf_A(u) \pm \operatorname{sgn}(\beta+u)\, h(u)]\,\mathrm{d}u. \tag{2.22}$$

2.2. *Numerical solutions of the system of integral equations*

We studied numerically the solutions of the pair of integral equations for $f_A(\xi)$ and $h(\xi)$, given by (2.13) and (2.19). Double-precision calculations using the NAG nonlinear system solver C05NBF with the integration routine D01GAF were used on N equidistributed points on the interval $(-L-\beta, L+\beta)$. The source strength Q was obtained simultaneously as the solution of an $(N+1)$th equation. Table 1 summarizes our findings, and includes the asymptotic results to be discussed in §4.

The most prominent feature of these computations is the tendency for $\alpha^{(+)}/\alpha^{(-)}$ to become small as β becomes large. Ultimately, of course, the cat's eyes disappear and (1.27) is obtained, but it is remarkable how quickly this behaviour is realized as β increases. The physical result is that the dominant induction occurs for a mean field perpendicular to the axis of the cat's eyes (at an angle 45° to the Ox axis), there being very little effect on fields parallel to the eyes. This is of course a manifestation of the stretching out of field lines in the channels, which occurs only if the mean field crosses the axis of the eyes.

In view of (1.27) it might be expected that $\det(\alpha)$ would decrease with β, but it is evident from table 1 that this is not the case. Since (cf. §5) the usual α^2-dynamo effect depends upon the size of $\det(\alpha)$ rather than on the magnitude of any one entry in the matrix (and in particular vanishes for the singular matrix (1.27)), this property of the cat's-eye flows is an important one and is the main result of this paper insofar as dynamo action is concerned. However, in order to reliably calculate $\det(\alpha)$ at large β we must accurately determine $\alpha^{(+)}$ and this becomes increasingly difficult to do numerically because, relative to the size of the channel, the magnetic boundary layer width decreases, leading to a finer magnetic field structure. This difficulty highlights the importance of an asymptotic theory for large β. The asymptotic results given in table 1 support the numerical results and it will follow from the formulas given in §4

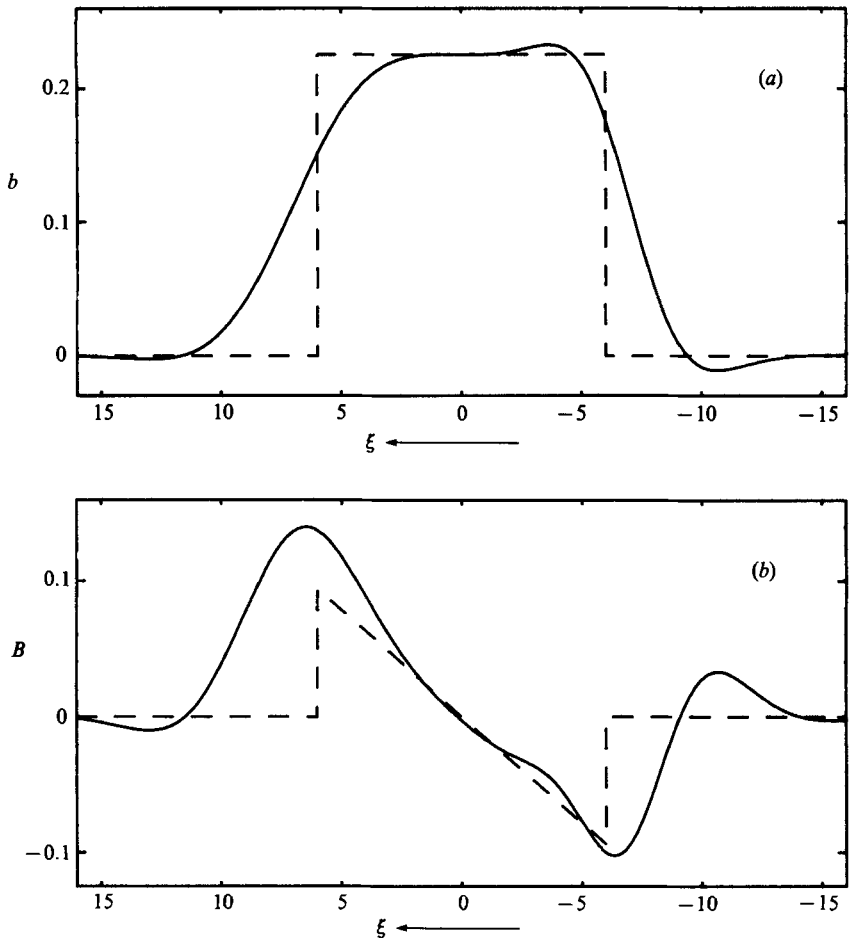

FIGURE 3 (a, b). For caption see next page.

that det $(\boldsymbol{\alpha})$ actually increases linearly with β for large β. We shall look more closely at the accuracy of the computed alpha-effect in §4.

We show b and B for $\beta = 6$ in figure 3. One sees in these figures the mainstream channel solutions emerging, bounded by magnetic layers. They carry magnetic flux b with a nearly uniform profile in the aligned case (see figure 3a), but with a nearly uniform *shear* in the perpendicular case (see figure 3c). Indeed, the results of §§3 and 4 below show that, for large β and within the channels, (2.13) and (2.19) are solved approximately by

$$[Q,b,B] \approx \begin{Bmatrix} \left[\dfrac{\sqrt{2\pi}}{\beta}, \dfrac{\pi}{2\beta}, 0\right], & \text{parallel} \\ [\sqrt{2\pi}\beta, \tfrac{1}{2}\xi\pi, \tfrac{1}{4}\pi(\xi^2-\beta^2)], & \text{perpendicular} \end{Bmatrix} \quad \text{case} \quad (\beta \gg 1). \quad (2.23a, b)$$

Only the first entry Q is dependent on the nature of the magnetic boundary layer (see §§4.2, 4.3); the other entries b and B are independent of it. Improved entries for B, incorporating boundary-layer contributions, are given in §4 (cf. (4.32b) and (4.47b)). The lowest-order results yield the alpha-matrix

$$-K^{-1}R^{\frac{1}{2}}\boldsymbol{\alpha} = \tfrac{1}{3}\beta^3\boldsymbol{I}^{(-)} \quad (\beta \gg 1). \quad (2.24)$$

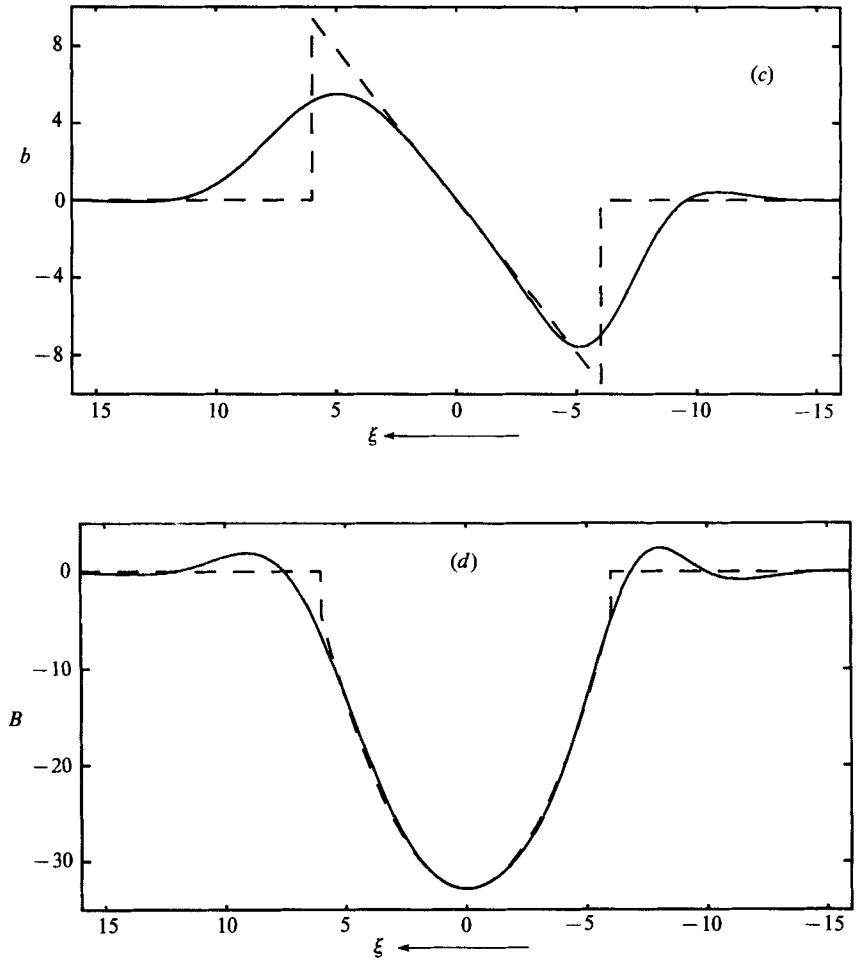

FIGURE 3. Terminal profiles, upon arrival at the point $P:(\pi,\pi)$ in figure 2(*a*), for the case $\beta = 6$. Positive and negative ξ correspond to flow on the left and right of the channel, respectively. The functions b and B, defined by (2.6) and (2.14), are plotted on (*a*) and (*b*) for the parallel field case ($\bar{\boldsymbol{B}}_{\mathrm{H}} = \boldsymbol{i}^{(+)}$) and on (*c*) and (*d*) for the perpendicular field case ($\bar{\boldsymbol{B}}_{\mathrm{H}} = \boldsymbol{i}^{(-)}$). The dashed lines are the complete ($\beta \gg 1$) mainstream solutions, as derived in §4. For these computations we adopted $N = 121$, $L = 24$, but only those parts of the solution with $|\xi| \leqslant 16$ are plotted.

In figure 3 the dashed lines superimposed on the calculated profiles show the asymptotic results for (b,B), obtained for large β and given by the results of §4.

We conclude from these studies at large β that the first-order expressions (2.23) give good approximations when β exceeds 6, while the boundary-layer corrections make the answers reliable down to $\beta = 1.5$ approximately.

3. Analysis of the finite channel

We now turn to the expansion for large R for fixed $\delta > 0$, at points that are not on separatrices.

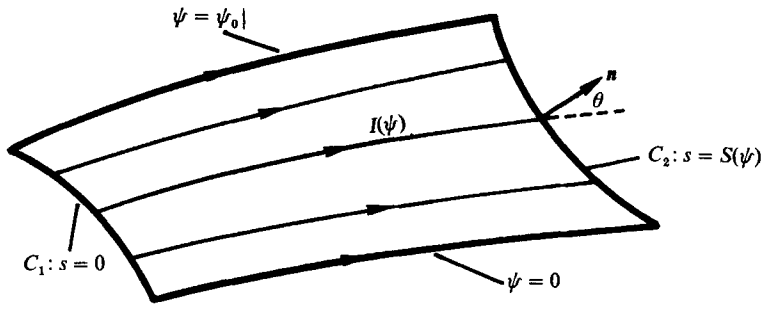

FIGURE 4. The geometry of a finite channel.

3.1. *Expansion for small diffusivity*

A direct attack on (1.3) and (1.14) for large R and fixed $\delta > 0$ must be confined to the mainstream regions away from boundary layers, and so the analysis will determine solutions uniquely only up to the first non-vanishing contribution from matching with the boundary layers. (The question of matching is considered in §4.)

We first study (1.3) for a general domain, within which diffusive effects are assumed to be small. The Prandtl–Batchelor theory we use is well known from the corresponding analysis of vorticity for nearly inviscid flows. For a summary and references to the literature see Lagerstrom (1975).

Consider the family of streamlines $I(\psi), 0 < \psi < \psi_0$ shown in figure 4. Here the streamlines connect two arcs $C_{1,2}$ where we assume that the values of A are given. For analysing this problem we may take ψ and the arclength s measured from C_1 to be the independent variables, where $s = S(\psi)$, say, on C_2. We shall try to solve

$$q\frac{\partial A}{\partial s} - R^{-1}\nabla^2 A = 0 \tag{3.1}$$

in the form

$$A = R^{\mu}(A_0 + R^{-1}A_1 + O(R^{-2})), \tag{3.2}$$

where R^{μ} is a scale factor; the exponent μ will be chosen as part of the solution and will depend upon the mean field orientation. The assumption (3.2) is a very restricted one based solely upon the form of (3.1) and our intention is to seek only a full determination of A_0. In general the matching with the boundary layers (as in §4) leads to terms of intermediate orders in (3.2), probably beginning with one of order $R^{\mu-\frac{1}{2}}$ and possibly to more involved orders containing $\ln R$. The first intermediate term is necessarily a solution of the homogeneous heat equation, however, and so is independent of the present computation of A_0.

Substituting (3.2) into (3.1), we see from the terms of order R that A_0 is a function of ψ alone, and from the terms of order unity that

$$q\frac{\partial A_1}{\partial s} = \nabla^2 A_0(\psi). \tag{3.3}$$

Thus

$$\int_{I(\psi)} q^{-1}\nabla^2 A_0 \,\mathrm{d}s = A_1(S(\psi), \psi) - A_1(0, \psi) \equiv [A_1]. \tag{3.4}$$

The left-hand side of (3.4) may be transformed to give

$$[A_1] = \frac{\partial}{\partial \psi}\iint_{R_\psi} q^{-1}\nabla^2 A_0 \,\mathrm{d}s\,\mathrm{d}\psi, \tag{3.5}$$

where R_ψ is the domain bounded by $I(\psi)$, the lowest streamline $I(0)$, and the arcs $C_{1,2}$. Since an area element $\mathrm{d}x\,\mathrm{d}y$ transforms to $q^{-1}\,\mathrm{d}s\,\mathrm{d}\psi$ we see that the right-hand side may be evaluated using the divergence theorem to obtain

$$[A_1] = \frac{\partial}{\partial\psi}\left(\gamma(\psi)\frac{\partial A_0}{\partial\psi}\right) + \Delta(\psi), \tag{3.6}$$

where

$$\gamma(\psi) = \int_{I(\psi)} \boldsymbol{u}\cdot\mathrm{d}\boldsymbol{s}, \tag{3.7a}$$

$$\Delta(\psi) = \frac{\partial A_0}{\partial\psi}(S(\psi),\psi)\tan\theta_2 - \frac{\partial A_0}{\partial\psi}(0,\psi)\tan\theta_1 \tag{3.7b}$$

and $\theta_{1,2}$ is the angle between the normal on $C_{1,2}$ and the tangent vector to a streamline (see figure 4).

Given the functions $\Delta(\psi)$ and $[A_1](\psi)$, (3.6) is an equation for $A_0(\psi)$, whose solution is uniquely determined by supplying two boundary conditions. The latter are typically obtained as matching conditions across thin diffusive layers.

Turning to the field B, and adopting an expansion of the form (3.2) with the same μ, we see from (2.1b) that B_0 is independent of s and that

$$q\frac{\partial B_1}{\partial s} = \nabla^2(B_0 - A_0), \tag{3.8}$$

which can be solved in the same way as (3.3).

Of course the expansion (3.2), augmented by the intermediate terms mentioned above and continued indefinitely as an asymptotic series in $R^{-\frac{1}{2}}$, can be obtained by systematic matching with the boundary layers. If the resulting expansion were then simultaneously expanded for small δ, the terms could be recast as an expansion in β^{-1}. It is more efficient, however, to recover the channel solutions for large β directly from the boundary-layer solution, as we show in §4 below.

3.2. *Application to the channel*

We now apply these results to the particular flow (1.1) and restrict attention mainly to the channels, $-\delta < \psi < \delta$. In order to utilize the result (3.6) we take C_1 as some arc across the primary channel and relate C_2 to it by the transformation $(x,y)\to(x+\pi, y+\pi)$ (e.g. A_1 and A_5 in figure 2a). The periodicity of the flow and the corresponding magnetic field implies that $\Delta = 0$ in all applications. To calculate γ it is convenient to express the horizontal components of the velocity in the form

$$\boldsymbol{u}_{\mathrm{H}} = (U(x,\psi), U(y,\psi)), \tag{3.9a}$$

where

$$U(\tau,\psi) = [\delta^2 - \psi^2 + (1-\delta^2)\sin^2\tau]^{\frac{1}{2}}. \tag{3.9b}$$

Here we have transformed both components of (3.9a) in order to make the stream function a coordinate in each case. It follows immediately from (3.7a) and (3.9) that

$$\gamma(\psi) = 2\int_0^\pi U(\tau,\psi)\,\mathrm{d}\tau \quad (-\delta < \psi < +\delta), \tag{3.10}$$

which introduces the geometry of the flow (1.1) into the present theory. The limiting

forms of U and γ, which occur when either the cat's eyes almost fill the squares $D_{m,n}(\delta \ll 1)$ or disappear ($\delta = 1$), are

$$U \approx \begin{cases} \sin\tau, \\ (1-\psi^2)^{\frac{1}{2}}, \end{cases} \quad \gamma \approx \begin{cases} 4, \\ 2\pi(1-\psi^2)^{\frac{1}{2}}, \end{cases} \tag{3.11a, b}$$

respectively.

The theory is modified slightly within the cat's eyes. There we consider closed streamlines ($C_1 \equiv C_2$) so that again $\Delta = 0$ but in addition we necessarily have $[A] = 0$. It follows that (3.6) simplifies and can be integrated once giving

$$\gamma(\psi)\frac{\partial A_0}{\partial \psi} = \text{constant}. \tag{3.12}$$

Since γ vanishes at the O-type stagnation point of the horizontal motion $\boldsymbol{u}_{\mathrm{H}}$ at the centre of the eye, the constant in (3.12) is zero, implying that A_0 is independent of ψ and therefore constant everywhere on the eye $\delta < |\psi| < 1$. Of course, an iterative solution of (3.1) then reveals that A is constant to all orders and deviates only in the magnetic layers near the edges of the eyes. A similar result holds for B. The resulting mainstream eye values for A and B are given by (2.2) and the values of A neighbouring the primary channel are illustrated in figure 2(*a*).

When the magnetic field is parallel to the channels, $\boldsymbol{B}_{\mathrm{H}} = \boldsymbol{i}^{(+)}$, the choice $\mu = 0$ in (3.2) is appropriate. A match with the cat's-eye solution on either side of the *primary* channel is achieved when $A_0(\delta) = 0$ and $A_0(-\delta) = -\pi$. Since there is no secular change of A down the channel we have $[A_1] = 0$. Integration of (3.6) subject to our two boundary conditions at $\psi = \pm\delta$ yields

$$A_0 = -\tfrac{1}{2}\pi\left[\int_{\psi}^{\delta} \frac{\mathrm{d}\psi}{\gamma(\psi)}\right]\left[\int_{0}^{\delta} \frac{\mathrm{d}\psi}{\gamma(\psi)}\right]^{-1}, \tag{3.13}$$

with the limiting values

$$A_0 \approx \begin{cases} \dfrac{\pi}{2\delta}(\psi - \delta) & (\delta \ll 1), \\ y - x & (\delta = 1). \end{cases} \tag{3.14a, b}$$

The small-δ result yields the middle entry of (2.23*a*), while the result for $\delta = 1$ recovers the mean magnetic field $\bar{\boldsymbol{B}}_{\mathrm{H}}$, which remains aligned to the unidirectional flow $\boldsymbol{u}_{\mathrm{H}}$.

The more interesting case occurs when the mean magnetic field is perpendicular to the channels, $\boldsymbol{B}_{\mathrm{H}} = \boldsymbol{i}^{(-)}$. In this case the secular increase of $\boldsymbol{A}$ down the channel implies that the choice $\mu = 1$ in conjunction with $[A_1] = 2\pi$ is appropriate. It means that a field of order R is required to make diffusion of order unity. This ordering, which is needed to make A change by an order-one amount along a streamline of the primary channel, is the source of the strong channel field realized by the cat's-eye flows. By the symmetry, $\partial A_0/\partial\psi$ (within the primary channel) is an odd function of ψ and so (3.6) integrates to

$$\gamma(\psi)\frac{\partial A_0}{\partial \psi} = 2\pi\psi. \tag{3.15}$$

Just as in the case of aligned fields considered above, we impose continuity of A_0 between channel and eye, which is a necessary consequence of the fact that the fluxes

within the magnetic boundary layers are fixed by the mean field to be of order unity, whereas a jump in A_0 implies a concentrated flux of order R. Since at leading order A_0 vanishes in the cat's eyes, the boundary conditions on (3.15) are $A_0(\pm\delta) = 0$. Consequently the integration of (3.15) yields

$$R^{-1}A \approx A_0 = 2\pi \int_{-\delta}^{\psi} \frac{\psi \, \mathrm{d}\psi}{\gamma(\psi)}, \tag{3.16}$$

with limiting values

$$A_0 \approx \begin{cases} \frac{1}{4}\pi(\psi^2 - \delta^2) & (\delta \ll 1), \\ \sin(y-x) & (\delta = 1). \end{cases} \tag{3.17a, b}$$

The small-δ result yields the middle entry of (2.23b), while the $\delta = 1$ result is consistent with (1.26b).

The calculation of B_0 from (3.8) proceeds in a similar way, but now the cat's-eye solutions (2.2b) imply that $[B] = 0$ in every case. The equation analogous to (3.6) integrates once giving

$$\gamma(\psi)\frac{\partial}{\partial\psi}(B_0 - A_0) = \text{constant}. \tag{3.18}$$

The solutions, which satisfy the boundary conditions at $\psi = \pm\delta$, are

$$B_0 = \begin{cases} 0, & \text{parallel case}, \\ A_0, & \text{perpendicular case}. \end{cases} \tag{3.19a, b}$$

In the case of small δ the result yields, with the help of (3.14a) and (3.17a), the final entries of (2.23a) and (2.23b) respectively. On the other hand, when $\delta = 1$, (3.19b) completes the solution (1.26b).

The channel contributions to the alpha-effect can now be calculated from the present limits using (1.21) (or (1.19)). We obtain

$$\pm R^{-\mu}\alpha^{(\pm)} \approx -\frac{1}{\pi}\int_{-\delta}^{+\delta}\left[\psi\frac{\partial A_0}{\partial\psi} - B_0\right]\mathrm{d}\psi, \tag{3.20}$$

where as in §2 the upper and lower signs refer to the cases of parallel ($\mu = 0$) and perpendicular ($\mu = 1$) mean magnetic fields respectively. In the parallel case, $\partial A_0/\partial\psi$ is even in ψ, while B_0 vanishes. It follows that

$$\alpha^{(+)} = 0. \tag{3.21}$$

On the other hand, for the perpendicular case (3.20) reduces, with the help of (3.15), to

$$R^{-1}\alpha^{(-)} = 8\int_0^{\delta} \frac{\psi^2 \, \mathrm{d}\psi}{\gamma(\psi)}, \tag{3.22}$$

with limiting values

$$R^{-1}\alpha^{(-)} \approx \begin{cases} \frac{2}{3}\delta^3 & (\delta \ll 1), \\ 1 & (\delta = 1). \end{cases} \tag{3.23a, b}$$

With (3.21) the small-δ result yields (2.24), while the $\delta = 1$ calculation is consistent with the exact result (1.27b).

The mainstream channel solution match with shear layers located at the streamlines $\psi = \pm\delta$. The resulting contribution to the alpha-effect needs to be included only when δ is small and β is not too large as we discuss in detail in the next Section. In the parallel field case they lead to the alpha-effect,

$$\alpha^{(+)} = O(R^{-\frac{3}{2}}\delta^{-2}) \quad (\delta \ll 1), \tag{3.24}$$

(see (4.32*a*) below) as $R \to \infty$ at small but fixed δ. This produces a surprisingly small induced current, of order $R^{-\frac{3}{2}}$, given that the integrand on the right of (3.20) is of order unity. In the perpendicular field case we see that, at the edges of the channel,

$$R\psi \frac{\partial A_0}{\partial \psi} = \tfrac{1}{2}\pi\beta^2. \tag{3.25}$$

This order of magnitude is maintained within the boundary layer of thickness order $R^{-\frac{1}{2}}$. Consequently the boundary-layer contribution to (3.20), which must be added to (3.22), is of order β^2. This contribution is seen in (4.47*a*), while additional contributions of the same order emerge from the mainstream vertical magnetic field, KB, which is modified by the presence of the boundary layers (see (4.41*b*) below).

4. Boundary-layer theory for large β

4.1. *Solution for non-interacting layers bounding a channel*

We turn attention again to the boundary-layer limit investigated in §2 but now consider the case $\beta \gg 1$, for which the boundary layers triggered at the corners stay close to the separatrices and the channel thickness is large compared with the boundary-layer thickness. In this limit the boundary-layer structure of §2 splits into the layers associated with the channel boundaries, together with an 'outer' solution valid within the channel $\delta - |\psi| \gg R^{-\frac{1}{2}}$. The basic assumption upon which the present calculation proceeds is that the solution near $\psi = \delta$ is not affected by the boundary layer on the opposite side of the channel (near $\psi = -\delta$). Our intention is to deal analytically with the boundary layers in the large-β limit and derive the asymptotic alpha-effect recorded in table 1. Our results will in effect provide all the higher-order corrections to the channel analysis of the last Section, arising from the presence of the diffusive layers, up to terms that represent the interaction of layers bounding a channel. Small differences between these analytic results and the tabulated values will persist, particularly at the smaller β, and must be attributed to layer interactions. Nevertheless we shall show that our basic assumption of independence of the layers appears to be reasonably well satisfied down to $\beta = 1.5$, this accuracy being a consequence of the rapid decay of the boundary-layer influence away from the separatrices. In fact the success of the method is probably a result of exponential decay with β of the contribution associated with boundary-layer interactions (see §4.4 below).

The mathematical apparatus set up in §2 continues to apply but we modify it to accommodate the assumption just mentioned. The main change is to extend the use of the Green-function solution (2.8*a*) from OP' to the entire separatrix OP ($0 < \sigma < 4$). We define $g_{A,B,C}$ as before by the values at $\sigma = 0_+$ (e.g. $g_A = b(0_+, \xi) - Q\delta(\xi - \beta)$) but the terminal values $f_{A,B,C}$ are now taken at $\sigma = 4_-$. The evolution of the ensuing integral in (2.8*a*), and of the boundary layer emanating from $(0_+, \beta)$, is simplified by the introduction of the stretched stream function

$$\zeta = \tfrac{1}{4}(\xi - \beta). \tag{4.1}$$

This leads to the boundary-layer form of the equation for A,

$$\pi^{\frac{1}{2}} f_A(\zeta) = \tfrac{1}{4} Q\, \mathrm{e}^{-\zeta^2} + \int_{-\infty}^{+\infty} g_A(u)\, \mathrm{e}^{-(\zeta-u)^2}\, \mathrm{d}u, \tag{4.2a}$$

while for C we have

$$\pi^{\frac{1}{2}} f_C(\zeta) = \int_{-\infty}^{+\infty} g_C(u)\, \mathrm{e}^{-(\zeta-u)^2}\, \mathrm{d}u. \tag{4.2b}$$

The secularity and symmetry results (2.5a, b), together with (2.4a), give

$$f_{A,C}(\zeta) = -\operatorname{sgn}(\zeta) g_{A,C}(\zeta) \tag{4.3}$$

for A and C. We now consider in detail the solution of the boundary-layer problem defined by (4.2) and (4.3). The structure of the boundary layer on the opposite side of the channel can then be inferred from the symmetry of the flow.

We shall solve (4.2), (4.3) by extending the Wiener–Hopf procedure used in S (Appendix) to the case $\beta > 0$.

Other, related heat-conduction problems have been solved with the Wiener–Hopf method. Stewartson (1968) determined the initial temperature of an infinite bar, such that after time T half of the bar has the initial temperature distribution, a problem that had been solved numerically by other workers. Benney & Bergeron (1969) studied the viscous layer bounding a row of cat's eyes at a critical layer. The Wiener–Hopf problem that arises there is closely related to the Stewartson (1968) problem, but is essentially different. The cat's-eye problem arises again at the critical layer of a Rossby wave, and Brown & Stewartson (1978) give a detailed analysis. For our problem, when β is large, the diagonal rows of cat's eyes do not interact, and each row is similar to a critical layer. Our analysis thus includes the Brown & Stewartson (1978, equations (3.18) and (3.19)) problem as a special case. Their problem corresponds to our homogeneous problem (4.2b), (4.3) for f_C with the boundary conditions (4.25) appropriate to the parallel case. Here, we also must solve the problem with the different boundary conditions (4.35) appropriate to the perpendicular case, as well as the inhomogeneous problem (4.2a), (4.3) for f_A. Nevertheless, the key functions $F_{\pm}(k)$, upon which our Wiener–Hopf solution (4.10) below is based, are derivable from their results. We indicate these derivations, using an alternative approach, in Appendix A.

We now define our Wiener–Hopf problem and give the solution. Details are relegated to Appendix A. The Wiener–Hopf method (see Noble 1958) relies on the use of the Fourier half-transforms

$$\hat{f}_+(k) = \int_0^\infty f(\zeta) \mathrm{e}^{\mathrm{i}k\zeta} \mathrm{d}\zeta, \quad \hat{f}_-(k) = \int_{-\infty}^0 f(\zeta) \mathrm{e}^{\mathrm{i}k\zeta} \mathrm{d}\zeta, \tag{4.4a, b}$$

Since the inverse transformation of $\hat{f}_+(k)$ necessarily vanishes for all $\zeta < 0$, $\hat{f}_+(k)$ must be analytic in the upper half of the complex k-plane, $\operatorname{Im}(k) > 0$. Likewise $\hat{f}_-(k)$ is analytic in the lower half, $\operatorname{Im}(k) < 0$. We use this subscript notation for other variables as well. Now the Fourier transforms of (4.2) and (4.3) yield

$$\hat{f}_A \equiv \hat{f}_{A+} + \hat{f}_{A-} = (\tfrac{1}{4}Q - \hat{f}_{A+} + \hat{f}_{A-}) \mathrm{e}^{-k^2/4}, \tag{4.5a}$$

$$\hat{f}_C \equiv \hat{f}_{C+} + \hat{f}_{C-} = (-\hat{f}_{C+} + \hat{f}_{C-}) \mathrm{e}^{-k^2/4}, \tag{4.5b}$$

which we rewrite in the form

$$\frac{\hat{f}_{A+}(k) - \frac{1}{8}Q}{F_+(k)} = -\frac{\hat{f}_{A-}(k) + \frac{1}{8}Q}{F_-(k)} [= F_A(k), \text{ say}], \tag{4.6a}$$

$$\frac{\hat{f}_{C+}(k)}{F_+(k)} = -\frac{\hat{f}_{C-}(k)}{F_-(k)} [= F_C(k), \text{ say}], \tag{4.6b}$$

where $F_{\pm}(k)$ are the functions (A 2b, c) defined in Appendix A with the properties

$$F_+(k) = O(k), \quad F_-(k) = O(k^{-1}) \quad \text{as} \quad k \to 0, \tag{4.7a}$$

$$F_+(k) \to 1 \quad \text{as} \quad \operatorname{Im}(k) \to +\infty, \quad F_-(k) \to 1 \quad \text{as} \quad \operatorname{Im}(k) \to -\infty. \tag{4.7b}$$

By construction the functions $F_\pm(k)$ are analytic and without zeros in the upper and lower halves of the complex k-plane, except for the zero and pole identified by (4.7*a*). The singularities of $\hat{f}_\pm(k)$ at the origin are determined by the behaviour of $f(\zeta)$ as $\zeta \to \pm\infty$. For our application they are

$$[\hat{f}_{A+}, \hat{f}_{C+}] = O(1), \quad [\hat{f}_{A-}, \hat{f}_{C-}] = O(k^{-2}), \quad \text{as} \quad k \to 0. \tag{4.8a}$$

We also note from the definitions (4.4*a*) that

$$[\hat{f}_{A+}, \hat{f}_{C+}] \to 0 \quad \text{as} \quad \mathrm{Im}\,(k) \to +\infty, \quad [\hat{f}_{A-}, \hat{f}_{C-}] \to 0 \quad \text{as} \quad \mathrm{Im}\,(k) \to -\infty. \tag{4.8b}$$

It is now a consequence of the Wiener–Hopf method that the functions $F_A(k)$ and $F_C(k)$ in (4.6) have the form

$$F_A = -\tfrac{1}{8}Q\left(1+\frac{a}{\mathrm{i}k}\right), \quad F_C = \frac{d}{\mathrm{i}k}, \tag{4.9a, b}$$

where a and d are constants, as yet unknown. The corresponding half-transforms which define $f_A(\zeta)$ and $f_C(\zeta)$ are

$$\hat{f}_{A\pm} = \pm\tfrac{1}{8}Q\left[1-\left(1+\frac{a}{\mathrm{i}k}\right)F_\pm(k)\right], \quad \hat{f}_{C\pm} = \pm\frac{d}{\mathrm{i}k}F_\pm(k). \tag{4.10a, b}$$

Except for the values of the constants a and d the solution of the boundary-layer problem for non-interacting layers is complete. To fix their values, the boundary-layer solution must be matched with the mainstream solution. To leading order the mainstream solutions are given by (2.23), and we have seen in §3 that these may be derived from the finite-channel theory for small δ. Our present aim is to incorporate these solutions into the formal expansion for large β, and thereby obtain improved mainstream solutions which include all boundary-layer contributions excluding interactions.

The needed matching may be achieved by decomposing all dependent variables into two parts, e.g.

$$A = A^{\mathrm{MS}} + A^{\mathrm{BL}}, \tag{4.11}$$

where A^{MS} is the mainstream solution and A^{BL} is the boundary-layer correction which vanishes as $|\xi-\beta| \to \infty$. We have seen that the magnetic flux is expelled from the cat's eyes, so by (2.3)

$$b^{\mathrm{MS}}(\sigma, \xi) = B^{\mathrm{MS}}(\sigma, \xi) = 0 \quad (0 < \sigma < 4, \xi-\beta > 0). \tag{4.12}$$

This means that the mainstream contributions to $f_A(\zeta)$ and $f_C(\zeta)$ are non-zero only for $\zeta < 0$. Consequently the Fourier transforms of their boundary-layer contributions are

$$\hat{f}^{\mathrm{BL}}(k) = \hat{f}_+(k) + \hat{f}_-(k) - \hat{f}_-^{\mathrm{MS}}(k), \tag{4.13}$$

since $\hat{f}_+^{\mathrm{MS}}(k) = 0$. This decomposition provides the key to our matching procedures because the vanishing of $f^{\mathrm{BL}}(\zeta)$ as $|\zeta| \to \infty$ implies that $\hat{f}^{\mathrm{BL}}(k)$ is analytic at $k = 0$. It then follows that the singularities of $\hat{f}_-(k)$ must be identical to those of $\hat{f}^{\mathrm{MS}}(k)$, thus fixing the constants a and d in (4.10). The nature of the resulting solutions depends significantly upon the orientation of the mean magnetic field, as we have seen in the preceding Sections. We therefore treat the parallel and perpendicular cases separately in the next two Subsections.

4.2. *The parallel case,* $\bar{\boldsymbol{B}}_{\mathrm{H}} = \hat{\boldsymbol{i}}^{(+)}$

In this case the mainstream value of the magnetic potential within each of the cat's eyes is

$$A^{\mathrm{MS}} = (n-m)\pi \quad \text{on} \quad D_{m,n}. \tag{4.14}$$

The symmetry about the centre of the *primary* channel implies that

$$A^{\mathrm{MS}}(\sigma, 0) = -\tfrac{1}{2}\pi \tag{4.15}$$

and so we deduce from (2.1a) that $\partial^2 A^{\mathrm{MS}}/\partial\xi^2 = 0$. Integration gives

$$b^{\mathrm{MS}} = b_0, \tag{4.16}$$

where $b_0 (= \partial A^{\mathrm{MS}}/\partial\xi)$ is a constant. Further integration of (4.16) and (4.14) then recovers our lowest-order channel field

$$b_0 \beta = \tfrac{1}{2}\pi + O(\beta^{-1}) \tag{4.17}$$

(see (3.14a)). The error of order β^{-1} anticipates boundary-layer corrections, and the complete asymptotic result, which ignores at most exponentially small terms (cf. §4.4), is given in (4.30) below.

Since both $\partial A^{\mathrm{MS}}/\partial\sigma$ and $\partial B^{\mathrm{MS}}/\partial\sigma$ are zero, (2.1b) implies that $\partial^2 B^{\mathrm{MS}}/\partial\xi^2 = 0$ also. Thus, using the symmetry once more, we obtain

$$B^{\mathrm{MS}} = B_0' \xi, \tag{4.18}$$

where $B_0' (= \partial B^{\mathrm{MS}}/\partial\xi)$ is a constant which remains to be determined. According to the channel solution (3.19a), B_0' must vanish at lowest order. It is, however, the non-zero value of order β^{-2} induced by boundary-layer corrections that controls the magnitude of the alpha-effect, as we shall see explicitly in (4.24) below.

Once our solution is found the magnitude of the alpha-effect defined by (2.20) may be calculated. To do this we need to follow the variation of E in the channel. It is therefore convenient to treat both boundary layers and channel simultaneously, and we introduce

$$E_+ = \frac{1}{\pi}\int_0^\infty (\xi b - B)\,\mathrm{d}\xi, \quad E_- = \frac{1}{\pi}\int_{-\infty}^0 (\xi b - B)\,\mathrm{d}\xi \tag{4.19a, b}$$

$$E = E_+ + E_-. \tag{4.19c}$$

Differentiating (4.19a) with respect to σ and using (2.1) and (4.18) gives

$$\pi\frac{\mathrm{d}E_+}{\mathrm{d}\sigma} = \left[\xi\,\frac{\partial b}{\partial\xi} - \frac{\partial B}{\partial\xi}\right]_{\xi=0}^{\xi=\infty} = B_0', \tag{4.20}$$

Integrating this expression with respect to σ, there results

$$\pi E_+ = B_0'(\sigma - 2) \quad (0 < \sigma < 4), \tag{4.21}$$

where the constant of integration has been chosen so that the right-hand side conforms to the symmetry by being antisymmetric about the midpoint $\sigma = 2$. Note that the integral (4.21) involves only the layer at $\psi = \delta$ and the half-channel $\psi > 0$. On the other side of the channel the boundary layer is discontinuous on the bounding streamline at the point P'. The contribution analogous to (4.21) from that half is

$$\pi E_- = \begin{cases} -B_0'\sigma & (0 \leqslant \sigma < 2), \\ -B_0'(\sigma - 4) & (2 < \sigma \leqslant 4), \end{cases} \tag{4.22}$$

and so the total contribution from the channel is

$$\pi E = \begin{cases} \pi E_{OP'} = -2B_0' & \text{on } OP', \\ \pi E_{P'P} = 2B_0' & \text{on } P'P. \end{cases} \tag{4.23}$$

The result is consistent with (2.20), which confirms the symmetry (4.21) and yields

$$R^{\frac{1}{2}}\alpha^{(+)} = \frac{2B_0'}{\pi}. \tag{4.24}$$

Our mainstream solutions (4.12), (4.16) and (4.18) define

$$f_A^{\mathrm{MS}}(\zeta) = f_C^{\mathrm{MS}}(\zeta) = 0 \quad (\zeta > 0), \tag{4.25a}$$

$$f_A^{\mathrm{MS}}(\zeta) = b_0, \quad f_C^{\mathrm{MS}}(\zeta) = (4B_0' - 2b_0)\,\zeta + B_0'\beta \quad (\zeta < 0), \tag{4.25b}$$

and they have the Fourier transforms

$$\hat{f}_{A-}^{\mathrm{MS}}(k) = \frac{b_0}{\mathrm{i}k}, \quad \hat{f}_{C-}^{\mathrm{MS}}(k) = -\frac{4B_0' - 2b_0}{(\mathrm{i}k)^2} + \frac{B_0'\beta}{\mathrm{i}k}, \tag{4.26}$$

defined in the first instance for $\mathrm{Im}\,(k) < 0$. As explained above, the singularities at $k = 0$ must be identified wth those of $\hat{f}_{A-}(k)$ and $\hat{f}_{C-}(k)$ as defined by (4.10). The singularities of these functions at $k = 0$ are given by (A 9). We equate the coefficients of $(\mathrm{i}k)^{-2}$ and $(\mathrm{i}k)^{-1}$ in (A 9) and (4.26) and obtain

$$a = 0, \quad Q/\sqrt{8} = b_0, \quad \sqrt{8}d = 4B_0' - 2b_0, \quad \sqrt{8}d\Gamma = -B_0'\beta. \tag{4.27}$$

Finally the magnetic flux conditions (4.14), (4.15) give

$$\int_0^\infty b\,\mathrm{d}\xi = \tfrac{1}{2}\pi, \tag{4.28}$$

from which the boundary-layer correction to (4.17) may be obtained:

$$\tfrac{1}{2}\pi - b_0\beta = 4\int_{-\infty}^{+\infty} b^{\mathrm{BL}}\,\mathrm{d}\zeta = 4\hat{f}_A^{\mathrm{BL}}(0). \tag{4.29a}$$

Use of (4.13), the first of (4.27), and (A 9*a*, *b*) gives

$$4\hat{f}_A^{\mathrm{BL}}(0) = \sqrt{2}Q\Gamma. \tag{4.29b}$$

The four unknowns Q, d, b_0 and B_0' are thus determined from the last three expressions in (4.27) and (4.29). The leading-order approximation to Q gives the first entry in (2.23*a*).

The main results are that

$$b_0 = \frac{\frac{1}{2}\pi}{\beta + 4\Gamma}, \quad B_0' = \frac{2\Gamma b_0}{\beta + 4\Gamma}. \tag{4.30}$$

Comparison of (4.30) with the zeroth-order result (4.17) shows that the boundary layer effectively increases the scaled channel flux by the amount

$$4\Gamma = 0.9653\ldots. \tag{4.31}$$

This is a measure of the boundary-layer 'displacement thickness'. The interesting feature of the expression for B_0' is that even its lowest-order value, $\pi\Gamma/\beta^2$, depends upon the boundary-layer solution, and so, unlike b_0, cannot be obtained from the

finite channel theory of §3. Moreover it is the small vertical magnetic field $KB_0'\xi$ which determines the alpha-effect defined by (4.24). It yields

$$R^{\frac{1}{2}}\alpha^{(+)} = \frac{2\Gamma}{(\beta+4\Gamma)^2}. \tag{4.32a}$$

From (4.16)–(4.18) and (4.30) we obtain the full mainstream solutions, which incorporate all non-interactive boundary-layer corrections into (2.23a), in the form

$$[Q, b, B] \approx \left[\frac{\sqrt{2\pi}}{\beta}, \frac{\pi}{2\beta}, \frac{\pi\xi}{(\beta+2\Gamma)^2}\right], \text{ parallel case}, \tag{4.32b}$$

which are used to draw the dashed lines in figure 3(a, b).

4.3. *The perpendicular case*, $\bar{\boldsymbol{B}}_{\mathrm{H}} = \boldsymbol{i}^{(-)}$

In this case the magnetic potential takes the values

$$A^{\mathrm{MS}} = (n+m)\pi \quad \text{on} \quad D_{m,n}. \tag{4.33}$$

Consequently, the value of A at the edge of the channels increases secularly and, over the section OP, A increases by 2π. The appropriate solution of (2.1a) is therefore

$$A^{\mathrm{MS}} = \tfrac{1}{2}\pi(\sigma-2)+A_0+\tfrac{1}{4}\pi\xi^2, \quad b = \tfrac{1}{2}\pi\xi, \tag{4.34a}$$

where A_0 is a constant. There is no secular variation of the z-component of the magnetic field and the required symmetric solution of (2.1b) is

$$B^{\mathrm{MS}} = B_0+\tfrac{1}{4}\pi\xi^2, \tag{4.34b}$$

where B_0 is a constant.

The mainstream solutions (4.12) and (4.34) define

$$f_A^{\mathrm{MS}}(\zeta) = f_C^{\mathrm{MS}}(\zeta) = 0 \quad (\zeta > 0), \tag{4.35a}$$

$$f_A^{\mathrm{MS}}(\zeta) = \pi(2\zeta+\tfrac{1}{2}\beta), \quad f_C^{\mathrm{MS}}(\zeta) = \pi\beta\zeta+\tfrac{1}{4}\pi\beta^2+B_0 \quad (\zeta < 0). \tag{4.35b}$$

As in the previous case we have the Fourier transforms

$$\hat{f}_{A-}^{\mathrm{MS}}(k) = -\frac{2\pi}{(\mathrm{i}k)^2}+\frac{\pi\beta}{2\mathrm{i}k}, \tag{4.36a}$$

$$\hat{f}_{C-}^{\mathrm{MS}}(k) = -\frac{\pi\beta}{(\mathrm{i}k)^2}+\frac{\frac{1}{4}\pi\beta^2+B_0}{\mathrm{i}k}. \tag{4.36b}$$

As before we equate coefficients in (4.36) and (A 9) to obtain

$$aQ/\sqrt{8} = 2\pi, \quad (a\Gamma+1)Q/\sqrt{8} = \tfrac{1}{2}\pi\beta, \quad \sqrt{8}d = \pi\beta, \sqrt{8}d\Gamma = -\tfrac{1}{4}\pi\beta^2-B_0. \tag{4.37}$$

These relations fix the values of the unknown constants in $\hat{f}_A$ and $\hat{f}_C$,

$$a = \frac{-4}{\beta+4\Gamma}, \quad Q = \sqrt{2\pi}(\beta+4\Gamma), d = \pi\beta/\sqrt{8}, \tag{4.38a}$$

as well as the constant in (4.34b), namely

$$B_0 = -\tfrac{1}{4}\pi\beta(\beta+4\Gamma). \tag{4.38b}$$

Continuity of A at $\sigma = 4_-$ across $\xi = \beta$ implies that the jump in the value of A^{MS} defines the magnetic flux at that point in the boundary layer. By (4.34a) it is

$$-(\pi + A_0 + \tfrac{1}{4}\pi\beta^2) = 4\int_{-\infty}^{+\infty} b^{\mathrm{BL}}\,\mathrm{d}\zeta = 4\hat{f}_A^{\mathrm{BL}}(0), \tag{4.39}$$

and use of (4.13), (4.37) and (A 9) yields

$$A_0 = -\tfrac{1}{4}\pi(\beta + 4\Gamma)^2. \tag{4.40}$$

The results (4.38b) and (4.40) complete the mainstream solution (4.34) which becomes

$$A^{\mathrm{MS}} = \tfrac{1}{2}\pi(\sigma - 2) - \tfrac{1}{4}\pi[(\beta + 4\Gamma)^2 - \xi^2], \quad B^{\mathrm{MS}} = -\tfrac{1}{4}\pi[\beta(\beta + 4\Gamma) - \xi^2]. \tag{4.41a, b}$$

At leading order they reduce to the channel solutions (3.17a) and (3.19b) respectively, while the second of (4.38a) yields the first entry of (2.23b).

To evaluate the alpha-effect, we note from (2.20) that

$$R_{\mathrm{M}}^{\frac{1}{2}}\alpha^{(-)} = E_{OP'} = E_{P'P} = E = \text{constant}. \tag{4.42}$$

We set

$$E = E^{\mathrm{MS}} + E^{\mathrm{BL}}, \tag{4.43}$$

and evaluate separately the mainstream contribution

$$E^{\mathrm{MS}} = \frac{2}{\pi}\int_0^{\beta} (\xi b^{\mathrm{MS}} - B^{\mathrm{MS}})\,\mathrm{d}\xi = \tfrac{2}{3}(\beta + 3\Gamma)\beta^2, \tag{4.44}$$

and the boundary-layer contribution

$$\begin{aligned} E^{\mathrm{BL}} &= \frac{8}{\pi}\int_{-\infty}^{\infty} [(2\zeta + \beta) f_A^{\mathrm{BL}} - f_C^{\mathrm{BL}}]\,\mathrm{d}\zeta, \\ &= \frac{8}{\pi}\left[\left(\frac{2}{\mathrm{i}}\frac{\mathrm{d}}{\mathrm{d}k} + \beta\right)\hat{f}_A^{\mathrm{BL}} - \hat{f}_C^{\mathrm{BL}}\right]_{k=0}. \end{aligned} \tag{4.45}$$

The values of $\mathrm{d}\hat{f}_A^{\mathrm{BL}}/\mathrm{d}k$, $\hat{f}_A^{\mathrm{BL}}$ and $\hat{f}_C^{\mathrm{BL}}$ at $k = 0$ are given by the coefficients of the regular terms in the series expansions (A 9). Together with (4.38) they yield

$$E^{\mathrm{BL}} = 4\Gamma\beta(\beta + 4\Gamma) + \tfrac{16}{3}(2\Gamma^3 + \Lambda). \tag{4.46}$$

The sum of (4.44) and (4.46) gives the final result,

$$R_{\mathrm{M}}^{\frac{1}{2}}\alpha^{(-)} = \tfrac{2}{3}(\beta + \Gamma)(\beta + 4\Gamma)^2 + \tfrac{16}{3}\Lambda. \tag{4.47a}$$

The leading-order contribution recovers the channel solution (3.23a). Collecting the mainstream results we see from (4.41) that the boundary-layer additions to (2.23b) yield

$$[Q, b, B] = [\sqrt{2\pi\beta}, \tfrac{1}{2}\xi\pi, \tfrac{1}{4}\pi(\xi^2 - \beta(\beta + 4\Gamma))], \text{ perpendicular case}, \tag{4.47b}$$

which are used to draw the dashed curves in figures 3(c, d). Note in the case of B that the parabola does not meet the axis but rather terminates at $\xi = \pm\beta$ with the value $-\Gamma\beta\pi$.

4.4. *Error estimates*

The boundary-layer contributions of $f^{\mathrm{BL}}(\zeta)$ to our solutions can be obtained by inverting the transform of $\hat{f}^{\mathrm{BL}}(k)$ defined by (4.13). To evaluate the inversion formula

$$f^{\mathrm{BL}}(\zeta) = \frac{1}{2\pi}\int_{-\infty}^{\infty} \hat{f}^{\mathrm{BL}}(k)\,\mathrm{e}^{-\mathrm{i}k\zeta}\,\mathrm{d}k \tag{4.48}$$

it is sufficient to determine the poles of $F_{\pm}(k)$. It leads to power series expansions of the form

$$f^{\mathrm{BL}}(\zeta) = \left\{ \begin{array}{ll} \sum_{n=1}^{\infty} (f_{+}^{(2n-1)} \exp[((4n-2)\pi)^{\frac{1}{2}}(-1+\mathrm{i})\zeta] + \mathrm{c.c.}) & (\zeta > 0), \\ \sum_{n=1}^{\infty} (f_{-}^{(2n)} \exp[(4n\pi)^{\frac{1}{2}}(1+\mathrm{i})\zeta] + \mathrm{c.c.}) & (\zeta < 0), \end{array} \right\}, \quad (4.49a, b)$$

where the c.c. denotes complex conjugate and $f_{\pm}^{(m)}$ are complex constants linked to the residues of $F_{\pm}(k)$. Of course, (4.49) corresponds to the periodic solutions

$$A^{(m)} \exp\left[i\tfrac{1}{4} m\pi\sigma + (\pm 1 + \mathrm{i}) \frac{\pi}{\Delta_m} \xi \right], \quad (\Delta_m = (8\pi/m)^{\frac{1}{2}}) \qquad (4.50)$$

of the heat-conduction equation (2.1a), where $A^{(m)}$ is a complex constant and Δ_m is the half-ξ-period; the latter measures, at fixed σ, the ξ-distance between successive zeros of the function. Inside the cat's eyes ($\zeta > 0$), m is odd reflecting the symmetry implied by (2.5b). The lowest mode ($m = 1$) only repeats itself after one complete circuit of the cat's eye (σ-period = 8) and has the ξ-lengthscale

$$\Delta_1 = (8\pi)^{\frac{1}{2}} = 5.013\ldots, \quad \text{(cat's eye)}. \qquad (4.51a)$$

In the channel ($\zeta < 0$), m is even in accord with the secularity condition (2.5a). The lowest mode ($m = 2$) repeats itself after traversing one side of the cat's eye (σ-period = 4) and has the ξ-lengthscale

$$\Delta_2 = (4\pi)^{\frac{1}{2}} = 3.545\ldots, \quad \text{(channel)}. \qquad (4.51b)$$

Far from the separatrices $\xi = \pm\beta$ we expect the boundary-layer solutions to be dominated by the lowest modes, that is $m = 1$ in the cat's eyes and $m = 2$ in the channels. This effect is seen most readily from the profile of B in the parallel-field case ($\bar{\boldsymbol{B}}_{\mathrm{H}} = \boldsymbol{i}^{(+)}$) plotted on figure 3($b$). Here B comes entirely from the boundary layers on the separatrices. The figure clearly shows that the first two zeros of B, on the right and left of $\xi = -\beta = -6$, are separated by distances approximately equal to $\Delta_1 (\approx 5.0)$ and $\Delta_2 (\approx 3.5)$ respectively. It is also perhaps worth remarking at this point that on each of the figures 3(a, b, c, d) the boundary layers near $\xi = -\beta[\beta]$ on the right [left] of the graphs correspond to a σ-distance 2[4] from the previous corner at $P'[O]$. Consequently the boundary-layer structures illustrated are more intense near $\xi = -\beta$ than they are near $\xi = \beta$, because of the shorter σ-distance from the corner where the disturbance is triggered. These remarks also account for the asymmetry of the solutions about $\xi = 0$.

Our Wiener–Hopf analysis has relied on the assumption that the boundary layers on either side of the primary channel do not interact. According to (4.50) the dominant mode ($m = 2$) decreases by the factor $\exp(-2\pi\beta/\Delta_2)$ ($= \exp(-\pi^{\frac{1}{2}}\beta)$) across the channel of width 2β. This exponentially small factor is already less than 0.1 for the value $\beta = 1.5$ mentioned at the end of §2. The values of $R^{\frac{1}{2}}\alpha^{(\pm)}$ obtained by the numerical integration of (2.13) and (2.19) together with the corresponding asymptotic values determined by (4.32a) and (4.47a) are given in table 1. We plot their ratio in figure 5. The departure from unity in the value of the ratio is consistent with the decay factor $\exp(-\pi^{\frac{1}{2}}\beta)$ derived above.

Finally, we remark on the range $|u| < L + \beta$ used in the numerical integration of (2.13) and (2.19). Since the separatrices correspond to $u = \pm\beta$, the value L defines the ξ-length from the channel boundary into the cat's eyes, which is included in the integration. At that distance the dominant boundary-layer mode ($m = 1$) decreases

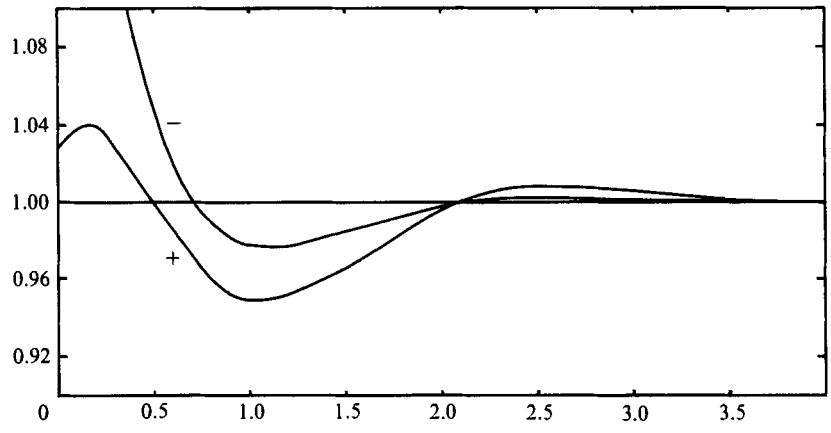

FIGURE 5. The ratio of the asymptotic to the numerical values of $R_{\frac{1}{2}}^{\frac{1}{2}}\alpha^{(\pm)}$ listed in table 1 are plotted versus β. The two sets of results are distinguished by the $\pm$ labels.

by the factor $e^{-\pi L/\Delta_1}$. For $L = 24$, the smaller of the two L listed in table 1, this factor is very small, $\approx 3 \times 10^{-7}$, and is therefore well into the asymptotic regime.

5. Discussion

In this paper we have obtained accurate values of the heat flux at fixed mean temperature gradient, and of the alpha-effect at fixed mean magnetic field, due to a family of two-dimensional steady Euler flows containing a periodic cat's-eye structure. The calculations have been carried out in the limit $R \to \infty$, for arbitrary positive $\delta R_{\frac{1}{2}}^{\frac{1}{2}}$. The stream function ψ given in (1.1) is characterized for $\delta > 0$ by the presence of channels which traverse the flow domain, as well as a periodic pattern of regions of closed streamlines. To the extent that general steady ψ will involve both bulk motion as well as 'trapped' eddies of closed streamlines, the method of analysis used here should be applicable to other steady two-dimensional flow fields, although the results we have presented depend heavily on the spatial periodicity. The boundary-layer limit uses only a few geometric properties of the flow (as in C) so that, so long as the vertical velocity component w is a function of ψ, the analysis near the streamsurfaces which separate islands and channels should proceed in a very similar way. Of course the connections between channels will determine the complexity of the associated boundary-layer problem. Other, more involved, extensions of the present work would break the condition that w be a function of ψ alone. Within this large family of flows the examples treated in the present paper stand out as among the simplest ones containing channels, because of the spatial periodicity and the very symmetric streamline pattern.

Applied to the thermal problem, our results show that problem of bulk transport at small diffusivity can be derived from the small-scale structures where molecular diffusivity remains active. We have also shown precisely how the boundary layers modify the mainstream solutions associated with zero diffusion. In the perpendicular case, and for the listed values in the range $2 \leqslant \beta \leqslant 4$, the bulk of the flux is carried by the channels, but there are still significant boundary-layer corrections. Since turbulent flows can diffuse a passive scalar in the limit of zero molecular diffusivity, asymptotic methods of this kind are of practical interest. Of course the restriction to steady flow precludes any direct relevance to turbulent diffusion, but it is interesting

that the *product* of diffusivities, $D^{(+)}D^{(-)}$ does have a finite limit for large R at fixed δ (the limit being $O(\delta^2)$, cf. (B 4) and (B 6)). Such a result could not have been anticipated from the solution at $\delta = 1$, using (1.25) and (1.27), and cannot be computed without the boundary-layer corrections.

In the magnetic problem the conclusions are similar, but there is the added feature of possible fast dynamo activity in the limit of infinite R. In a fast kinematic dynamo the boundary conditions must preclude external sources of magnetic energy, and the magnetic field (i.e. B and gradient of A) should grow, usually at an exponential rate, uniformly in the limit of infinite magnetic Reynolds number. (Of course turbulent diffusion, positive or negative, remains an interesting question in the magnetic problem, and could be studied with or without an associated dynamo effect.)

The present results do not provide a conclusive answer concerning the existence or non-existence of a fast dynamo for (1.1). Since our analysis of (1.1) parallels that of C for the case $\beta = 0$, the present computations of the alpha-effect do have some implications for the dynamo problem, as in S for the case of zero β. There, it was argued that the local analysis of the alpha-effect, wherein a uniform mean field is assumed, should also apply to a mean field which is periodic in z (and hence admissible in the context of kinematic dynamo theory), provided that the wavelength in z is large compared to the boundary-layer thickness $R^{-\frac{1}{2}}$. If this approach, mentioned towards the end of §1.4, is assumed to hold for $\beta > 0$ then the dispersion relation for the mean field will have the form

$$p = \pm(\det(\boldsymbol{\alpha}))^{\frac{1}{2}}n - R^{-1}n^2, \tag{5.1}$$

where n is the wavenumber for the mean field with growth rate p. Now from (4.32a) and (4.47a) we see that the asymptotic behaviour of $\det(\boldsymbol{\alpha})$ is, according to local theory,

$$K^{-2}\det(\boldsymbol{\alpha}) = \alpha^{(+)}\alpha^{(-)} = R^{-1}\tfrac{4}{3}\Gamma[\beta + \Gamma + 8\Lambda(\beta + 4\Gamma)^{-2}]. \tag{5.2}$$

Thus we have, for large β, and with the + sign in (5.1),

$$p \approx K(4\Gamma\beta/3R)^{\frac{1}{2}}n - R^{-1}n^2 \quad (\beta \gg 1). \tag{5.3}$$

A crucial question is the restriction that must be placed upon n, when β is large, to ensure the validity of local theory of the alpha-effect. One obvious limitation is the neglect of vertical diffusion in the mainstream channel flow. Solutions of the type (3.6) are valid only if the vertical lengthscale is large compared to the boundary-layer thickness, $n \ll \delta^{-1}$. This means that the unique maximum $\frac{1}{3}K^2\Gamma\beta$ of (5.3), which occurs when n is of order $(R\beta)^{\frac{1}{2}}(\gg \delta^{-1})$, is unacceptable. For Roberts' case $\delta = 0$, it was shown in S that the vertical advection of z-dependent mean magnetic field was the dominant process leading to the failure of the z-independent approximation. For our problem the vertical advection of horizontal magnetic field leads to a term like $K\psi(\partial A/\partial z)$ of order $K\delta nA$ on the left of (3.1). On forming the consistency condition (3.6), we must, therefore, include a term of order $KR\delta nA_0$. As a result, for large n, the channel solutions are confined to the boundary layers of width order $(KR\delta n)^{-\frac{1}{2}}$ in the neighbourhood of the separatrices. Neglect of this effect ceases to be valid when this width is as narrow as the channel width δ. Hence the upper bound on p imposed by the resulting estimate $n = O((KR\delta^3)^{-1})$ is, by (5.3), of order $K(\beta/R)^{\frac{1}{2}}n\,(=\beta^{-\frac{5}{2}})$. It means that, though increasing the channel width at fixed R strengthens $\det(\boldsymbol{\alpha})$, the upper bound on n decreases such that the product (at least for large β) decreases. Therefore, we do not expect fast dynamo action in the limit δ fixed, $R \to \infty$.

It is interesting that the difficulty comes from a factor of β which is missing from

(5.1) but present in the thermal problem in $\det(\boldsymbol{D})$. The latter quantity is $O(\beta^2/R)$. If this estimate were applied to α we would have fast dynamo activity for $n = O(1)$.

It is also of interest to fit the present results into the general conclusions of Moffatt & Proctor (1985). Their results established the importance of an $O(R^{-\frac{1}{3}})$ boundary-layer scale *throughout* a domain where a steady flow operates as a fast dynamo. In the present examples the relevant boundary-layer scales exist, but they are localized to the separatrices. In effect we might regard the above evidence against fast dynamo action as a consequence of this very local boundary-layer structure.

A separate issue, which involves the artificial device of making δ a function of R, is the question of fast dynamo action in the limit β fixed, $R \to \infty$. The answer to this question requires a three-dimensional analysis along the lines of the $\mu = O(1)$ theory mentioned in the penultimate paragraph of §1. We may reasonably expect that nearly fast dynamos similar to those given in S for $\delta = 0$ continue to exist and give the modes with maximum growth rates when $\delta \neq 0$. There is no suggestion that modes with significantly faster growth rate can be obtained with non-zero values of δ. Still, we may speculate that the modification of the flow in the corner regions (or some other small modification of the stream function), as proposed in S, can make the dynamo fast.

There is another line of attack, which could possibly use the model of the present paper to advantage in the construction of a fast dynamo. This involves abandoning the two-dimensionality of the flow by allowing a slow modulation in z. The idea is, of course, that three-dimensional steady flows offer easier access to fast dynamo action. What we have found in the present paper is a highly anisotropic alpha-effect once $\delta > 0$. Is it possible to modulate the direction of optimal regeneration on the wavelength of the growing mean field, in such a way that the action persists at infinite R? Soward & Childress (1986) have made a related proposal using three-dimensional flows of a different kind, but having a preferred axis of excitation. For a two-dimensional motion such as (1.1) the difficulty is to find a solenoidal three-dimensional extension that allows a local two-dimensional analysis of the alpha-effect. One possible approach is to introduce a rotation of axes and define a function

$$\tilde{\psi}(x, y, z) \equiv \psi(x\cos\theta + y\sin\theta, -x\sin\theta + y\cos\theta), \quad \theta = \epsilon z, \epsilon \ll 1, \tag{5.4}$$

where ψ is given by (1.1*b*). If we then use $\tilde{\psi}$ in (1.1*a*), the field $\boldsymbol{u}$ fails to be solenoidal. Although a correction of order ϵ is sufficient to remove the contribution to the divergence coming from the variation in z, the added term contains secular growth in x and y and is therefore unsatisfactory, a difficulty that is avoided by Soward & Childress (1986) by the use of a fully three-dimensional flow. By (4.47*a*), the largest induction is $O(R\delta^3)$ for small δ, which is, for fixed δ, far larger than the $O(1)$ which must be the largest possible growth rate for a fast dynamo. We must presume that, if a suitable three-dimensional extension of (1.1) could be found, the optimal growth rate would necessarily be reduced from this estimate by a factor R^{-1}. The main point seems to be that, even though the motion (1.1) is capable of intense excitation in a preferred direction (determined by the channel axes), the fast-dynamo issue remains just as delicate as in the case of vanishing channels.

We thank the anonymous referees for helpful comments concerning the presentation. We are also grateful to Dr S. Cowley for drawing our attention to the solution of the Wiener–Hopf problem given by Professors S. N. Brown and K. Stewartson. This research was begun under SERC grant number GR/D/7812.1 during June and July of 1986. The work was continued at New York University

under Grants NSF-DMS-831 2229 and NASA-NAGW-781. Part of the study was carried out at the 1987 Woods Hole Summer Study Program in Geophysical Fluid Dynamics. We thank the director of the 1987 Program, W. V. R. Malkus, for his encouragement and support.

Appendix A

Brown & Stewartson (1978) make use of integral representations of the Wiener–Hopf decomposition. An alternative method, used in S, is algebraic and relies on the identity

$$\frac{\sinh\zeta}{\zeta} = \prod_{n=1}^{\infty}\left[1+\left(\frac{\zeta}{n\pi}\right)^2\right]. \tag{A 1}$$

The functions $F_{\pm}(k)$ introduced in (4.6) satisfy

$$\frac{F_+(k)}{F_-(k)} = \tanh\left(\tfrac{1}{8}k^2\right). \tag{A 2a}$$

Their analyticity requirements are met by the factorization

$$F_+(k) = \frac{k\,\mathrm{e}^{\mathrm{i}\pi/4}}{k-2\pi^{\frac{1}{2}}\mathrm{e}^{-\mathrm{i}\pi/4}}\prod_{n=1}^{\infty}\left[\frac{(k-2(2n\pi)^{\frac{1}{2}}\mathrm{e}^{-\mathrm{i}\pi/4})(k+2(2n\pi)^{\frac{1}{2}}\mathrm{e}^{\mathrm{i}\pi/4})}{(k-2[(2n+1)\,\pi]^{\frac{1}{2}}\mathrm{e}^{-\mathrm{i}\pi/4})(k+2[(2n-1)\,\pi]^{\frac{1}{2}}\mathrm{e}^{\mathrm{i}\pi/4})}\right], \tag{A 2b}$$

$$F_-(k) = \frac{1}{F_+(-k)}, \tag{A 2c}$$

which also satisfies the boundary conditions at the origin (4.7a) and infinity (4.7b), as explained below. Brown & Stewartson (1978, Appendix A) define via their integral formulation the related functions

$$K_-(\omega) = \frac{\sqrt{8}}{\mathrm{i}k}\frac{1}{F_-(k)}, \quad K_+(\omega) = -\frac{\mathrm{i}k}{\sqrt{8}}\frac{1}{F_+(k)}, \tag{A 3}$$

where $\omega = k/\sqrt{2}$, with the properties

$$K_-(\omega)K_+(-\omega) = 1, \quad K_-(0) = K_+(0) = 1. \tag{A 4}$$

In addition they introduce the function $I(\omega)$ defined by

$$-\mathrm{i}I(\omega) = \tfrac{1}{2}\ln\left[K_+(\omega)K_-(\omega)\right], \tag{A 5a}$$

which by (A 4) is odd in $\omega\,[I(-\omega) = -I(\omega)]$. It may be used to give an alternative representation of $K_{\pm}(\omega)$, namely

$$-\ln\left[K_{\pm}(\omega)\right] = \pm\tfrac{1}{2}\ln\left[\frac{4}{\omega^2}\tanh\left(\frac{\omega^2}{4}\right)\right] + \mathrm{i}I(\omega). \tag{A 5b}$$

We outline briefly how the key properties of $F_{\pm}(k)$ are established from the definition (A 2). First, $K_+(0)$ can be evaluated directly from (A 2b) and (A 3) using the identity (A 1) with $\zeta = \frac{1}{2}\mathrm{i}\pi$. Secondly, to evaluate $F_+(k)$ as $\mathrm{Im}\,(k)\to+\infty$, we set $k = \mathrm{i}q$ and note that the dominant contribution comes from terms in the infinite product having n of order q^2. The logarithm of F_+ is an infinite sum which may be approximated by the integral

$$\ln\left[F_+(\mathrm{i}q)\right] \approx \tfrac{1}{4}\mathrm{i}\pi + \int_0^{\infty}\ln\left[\frac{[\frac{1}{2}\mathrm{e}^{-\mathrm{i}\pi/4}q+(2n\pi)^{\frac{1}{2}}][\frac{1}{2}\mathrm{e}^{\mathrm{i}\pi/4}q+(2n\pi)^{\frac{1}{2}}]}{[\frac{1}{2}\mathrm{e}^{-\mathrm{i}\pi/4}q+((2n+1)\,\pi)^{\frac{1}{2}}][\frac{1}{2}\mathrm{e}^{\mathrm{i}\pi/4}q+((2n-1)\,\pi)^{\frac{1}{2}}]}\right]\mathrm{d}n,$$

for large q. This result follows because the integrand vanishes when $q \ll n^{\frac{1}{2}}$, and only varies slowly as n is increased by unity, when $q = O(n^{\frac{1}{2}})$. Further approximations for large n lead to

$$\ln F_+(\mathrm{i}q) \approx \tfrac{1}{4}\mathrm{i}\pi - \frac{1}{2}\int_0^\infty \left[\frac{1}{(2n\pi)^{\frac{1}{2}} + \frac{1}{2}q\,\mathrm{e}^{-1\pi/4}} - \text{c.c.}\right] \mathrm{d}(2n\pi)^{\frac{1}{2}},$$

for large positive real values of q. where c.c. denotes complex conjugate. Integration gives the result $\ln F_+(\mathrm{i}q) \to 0$ as $\mathrm{Re}\,(q) \to +\infty$, which establishes (4.7*b*).

For our boundary-layer problem only the behaviour of $F_\pm(k)$ near $k = 0$ is needed. This is readily derived from (A 2) by expressing $\ln[F_\pm(k)]$ as an infinite sum and then expanding each term. This gives Brown & Stewartson's (1978, equation (A 18)) result for $I(\omega)$. The first few terms are

$$I(k/\sqrt{2}) = \Gamma k + \tfrac{1}{6}\Lambda k^3 + O(k^5) \quad \text{for } |k| \ll 1, \tag{A 6}$$

where

$$\Gamma = \frac{1}{(2\pi)^{\frac{1}{2}}}(1-2^{\frac{1}{2}})\,\zeta(\tfrac{1}{2}) = \sum_{n=1}^{\infty} \frac{(-1)^{n+1}}{(2\pi n)^{\frac{1}{2}}} = 0.241\,319\,644\,2\ldots, \tag{A 7a}$$

$$\Lambda = \frac{1}{(2\pi)^{\frac{3}{2}}}(1-2^{-\frac{1}{2}})\,\zeta(\tfrac{3}{2}) = \sum_{n=1}^{\infty} \frac{(-1)^{n+1}}{(2\pi n)^{\frac{3}{2}}} = 0.048\,581\,966\,61\ldots, \tag{A 7b}$$

and $\zeta(n)$ is the Riemann-Zeta function. Since the first term on the right of (A 5*b*) is of order k^4, we have the result

$$K_\pm(k/\sqrt{2}) = \mathrm{e}^{-\mathrm{i}I(k/\sqrt{2})} + O(k^4), \tag{A 8}$$

where $I(k/\sqrt{2})$ is given by (A 6) above.

Finally, the asymptotic behaviour of $\hat{f}_{A\pm}$ and $\hat{f}_{C\pm}$ for small k can be obtained from (A 6) and (A 8). It is

$$\hat{f}_{A+}(k) = \frac{Q}{8\sqrt{8}}[a + \sqrt{8} + (a\Gamma + 1)\,(\mathrm{i}k) + O(k^2)], \tag{A 9a}$$

$$\hat{f}_{A-}(k) = \frac{Q}{\sqrt{8}}\left[a\frac{1}{(\mathrm{i}k)^2} + \frac{(a\Gamma+1)}{\mathrm{i}k} + \left(\frac{1}{2}a\Gamma^2 + \Gamma - \frac{1}{\sqrt{8}}\right) + [\tfrac{1}{6}(\Gamma^3 - \Lambda)\,a + \tfrac{1}{2}\Gamma^2](\mathrm{i}k) + O(k^2)\right], \tag{A 9b}$$

$$\hat{f}_{C+}(k) = -\frac{d}{\sqrt{8}}[1 + O(k)], \tag{A 9c}$$

$$\hat{f}_{C-}(k) = -\sqrt{8}d\left[\frac{1}{(\mathrm{i}k)^2} + \Gamma\frac{1}{\mathrm{i}k} + \frac{1}{2}\Gamma^2 + O(k)\right]. \tag{A 9d}$$

Appendix B

We summarize here the application of the present methods to the problem of effective transport of a scalar field, as discussed in §1. To obtain the diffusion coefficients $D^{(\pm)}$ defined by (1.7) we need only set $B = 0$ in (1.19) and note the relationship (1.12) of $\bar{\boldsymbol{B}}_{\mathrm{H}}$ to $\boldsymbol{g}_{\mathrm{H}}$. For the parallel ($\boldsymbol{g}_{\mathrm{H}} = -\boldsymbol{i}^{(-)}$) and perpendicular ($\boldsymbol{g}_{\mathrm{H}} = \boldsymbol{i}^{(+)}$) cases, the boundary-layer theory of §2 thus leads, in place of (2.20), (2.21), to the results

$$\pm R^{\frac{1}{2}} D^{(\pm)} = \pm\tilde{E}_{P'P} = -\tilde{E}_{OP'}, \tag{B 1a}$$

where

$$\tilde{E} = \frac{1}{\pi}\int_{-\infty}^{+\infty} \xi b\,\mathrm{d}\xi. \tag{B 1b}$$

			$R^{\frac{1}{2}}D^{(+)}$		$R^{\frac{1}{2}}D^{(-)}$	
β	N	L	Numerical	Asymptotic	Numerical	Asymptotic
0	97	24	1.065	1.036	1.065	0.8180
0.5	103	25	0.7033	0.6825	1.783	1.567
1.0	101	24	0.5143	0.5088	3.146	3.048
1.5	107	25	0.4061	0.4056	5.506	5.513
2.0	105	24	0.3370	0.3372	9.168	9.209
2.5	111	25	0.2884	0.2886	14.36	14.39
3.0	109	24	0.2522	0.2522	21.29	21.30
3.5	115	25	0.2240	0.2240	30.20	30.20
4.0	113	24	0.2014	0.2014	41.33	41.32

TABLE 2. Numerical and asymptotic solutions for the diffusion coefficients

As before, the subscripts label the constant values taken on the two primary channel sections $P'P$ and OP', while the upper and lower signs still identify parallel and perpendicular respectively. The numerical values listed in table 2 are obtained from the result

$$\pm R^{\frac{1}{2}}D^{(\pm)} = -\frac{1}{\pi}\int_{-\infty}^{+\infty} u f_A(u)\,\mathrm{d}u \tag{B 2}$$

(cf. (2.22)).

The asymptotic results shown in table 2 are easily extracted from the calculations of §4 upon replacing E by $\tilde{E}$. For the parallel case the crucial modifications emerge from (4.20) which becomes

$$\pi\frac{\mathrm{d}\tilde{E}_+}{\mathrm{d}\sigma} = \left[\xi\frac{\partial b}{\partial \xi} - b\right]_{\xi=0}^{\xi=\infty} = b_0. \tag{B 3}$$

Hence B_0' in (4.24) is replaced by b_0 and so (4.32) is replaced by

$$R^{\frac{1}{2}}D^{(+)} = \frac{1}{\beta+4\Gamma}. \tag{B 4}$$

For the perpendicular case (4.44), (4.45) become

$$\tilde{E} = \frac{2}{\pi}\int_0^{\beta} \xi b^{\mathrm{MS}}\,\mathrm{d}\xi + \frac{8}{\pi}\int_{-\infty}^{+\infty} (4\zeta+\beta) f_A^{\mathrm{BL}}\,\mathrm{d}\zeta, \tag{B 5}$$

giving

$$R^{\frac{1}{2}}D^{(-)} = \tfrac{1}{3}(\beta+4\Gamma)^3 + \tfrac{32}{3}\Lambda \tag{B 6}$$

in place of (4.47a).

Finally, we remark that the numerical results quoted in table 2 are based upon the same numerical solutions as were used for table 1. The agreement between the numerical results and the asymptotic values therefore shows comparable accuracy.

REFERENCES

ANUFRIYEV, A. P. & FISHMAN, V. M. 1982 Magnetic field structure in the two-dimensional motion of a conducting fluid. *Geomag. Aeron.* **22**, 245–248.

BATCHELOR, G. K. 1956 On steady laminar flow with closed streamlines at large Reynolds number. *J. Fluid Mech.* **1**, 177–190.

BENNEY, D. J. & BERGERON, R. F. 1969 A new class of nonlinear waves in parallel flows. *Stud. Appl. Maths* **48**, 181–204.

BROWN, S. N. & STEWARTSON, K. 1978 The evolution of the critical layer of a Rossby wave. Part II. *Geophys. Astrophys. Fluid Dyn.* **10**, 1–24.

CHILDRESS, S. 1979 Alpha-effect in flux ropes and sheets. *Phys. Earth Planet. Inter.* **20**, 172–180 (denoted by 'C' in text).

CHILDRESS, S. & SOWARD, A. M. 1985 On the rapid generation of magnetic fields. In *Chaos in Astrophysics* (ed. J. R. Buchler, J. M. Perdang & E. A. Spiegel). NATO ASI Series C: Mathematical and Physical Sciences, Vol. 161, pp. 223–244.

DOMBRE, T., FRISCH, U., GREENE, J. M., HÉNON, M., MEHR, A. & SOWARD, A. M. 1986 Chaotic streamlines in the ABC flows. *J. Fluid Mech.* **167**, 353–391.

GALLOWAY, D. & FRISCH, U. 1986 Dynamo action in a family of flows with chaotic streamlines. *Geophys. Astrophys. Fluid Dyn.* **36**, 53–83.

LAGERSTROM, P. A. 1975 Solutions of the Navier–Stokes equation at large Reynolds number. *SIAM J. Appl. Maths* **28**, 202–214.

MOFFATT, H. K. 1978 *Magnetic Field Generation in Electrically Conducting Fluids.* Cambridge University Press.

MOFFATT, H. K. & PROCTOR, M. R. E. 1985 Topological constraints associated with fast dynamo action. *J. Fluid Mech.* **154**, 493–507.

NOBLE, B. 1958 *Methods Based on the Wiener–Hopf Technique.* Pergamon.

PERKINS, F. W. & ZWEIBEL, E. G. 1987 A high magnetic Reynolds number dynamo. *Phys. Fluids* **30**, 1079–1084.

PRANDTL, L. 1904 Über Flussigkeitsbewegung bei sehr kleiner Reibung. Proc. 3rd Intl Math. Cong. Heidelberg, pp. 484–491.

RHINES, P. B. & YOUNG, W. R. 1983 How rapidly is a passive scalar mixed within closed streamlines? *J. Fluid Mech.* **133**, 133–145.

ROBERTS, G. O. 1972 Dynamo action of fluid motions with two-dimensional periodicity. *Phil. Trans. R. Soc. Lond.* A **271**, 411–454.

SOWARD, A. M. & CHILDRESS, S. 1986 Analytic theory of dynamos. *Adv. Space Res.* **6**, 7–18.

SOWARD, A. M. 1987 Fast dynamo action in steady flow. *J. Fluid Mech.* **180**, 267–295 (denoted by 'S' in the text).

SOWARD, A. M. 1989 On dynamo action in a steady flow at large magnetic Reynolds number. *Geophys. Astrophys. Fluid Dyn.* (submitted).

STEWARTSON, K. 1968 On an integral equation. *Mathematika* **15**, 22–29.

ZEL'DOVICH, YA. B., RUZMAIKIN, A. A. & SOKOLOV, D. D. 1983 *Magnetic Fields in Astrophysics.* Gordon and Breach.